ABSTRACT

Complex Plasmas: A Computational Investigation of Self-Organizing Systems

Abbie Terrell

Director: Lorin S. Matthews, Ph.D.

Complex, or dusty, plasmas are ionized gases in which nanometer-to-micrometer sized microparticles are suspended. When dust particles are introduced in the plasma environment, they become negatively charged and interact with each other and the plasma background, self -organizing into stable structures. These far-from-equilibrium systems serve as a useful model system to study processes of self-organization in other complex systems. This thesis focuses on the numerical modeling of the Plasma Kristall-4 (PK-4) experiment, currently on board the International Space Station, through an N-body Molecular Dynamics simulation called DRIAD (Dynamic Response of Ions and Dust). It is shown that the dust cloud undergoes a phase transition that is studied quantitatively in multiple dimensions. The dust phase transition exemplifies the presence of analogous systems in physics, leading to a discussion of the relevance of studying physical phenomena though model systems.

APPROVED BY DIRECTOR OF HONORS THESIS:

____

Dr. Lorin Matthews, Physics

APPROVED BY THE HONORS PROGRAM:

____

Dr. Elizabeth Corey, Director

DATE:______________________________

COMPLEX PLASMAS:

A COMPUTATIONAL INVESTIGATION OF SELF-ORGAINIZING SYSTEMS

A Thesis Submitted to the Faculty of

Baylor University

In Partial Fulfillment of the Requirements for the

Honors Program

By

Abbie Terrell

Waco, Texas

May 2023

TABLE OF CONTENTS

PREFACE

This project began at least a year before it started, with a series of conversations that deeply affected my perspective on my own education and the remainder of my time at Baylor. Halfway through my sophomore year, when I found myself frustrated by my classes and uncertain of my academic goals, I reached out to two of the kindest professors I had taken classes with – an engineer, Dr. Jill Klentzman, and a physicist, Dr. Lorin Matthews. Their insight led me to the opportunity to join a research group.

Doing research for the first time changed me – I was once again curious, excited, and happy to carry out the day-to-day of my schoolwork. A future career in research seemed like something I genuinely wanted to do. Taking a deep-dive into a particular field was an opportunity to learn so much, so quickly. It required reading, writing, talking, and applying all that I had learned in my classes to think about general concepts within the scope of a particular field. Not only that, but it required looking at the work of other fields, understanding that no discipline is truly disconnected from others. I became interested in understanding the world through minutia, finding the connection between the smallest details and the larger scope. I loved that complex plasmas were "analogous systems," and could be used to understand self-organization of different kinds.

If I could do think project again, I would dive more deeply into the analogies present in physics, considering them from a scientific perspective as well as a philosophical one. My concluding chapter touches on some of these ideas – the importance of analogies for teaching, learning, and theorizing about new physics. My hope is that at least the first and last chapters can be interesting to the non-physicist.

ACKNOWLDGEMENTS

I am incredibly grateful to my thesis committee: Dr. Lorin Matthews, Dr. Truell Hyde, and Dr. Jill Klentzman. I owe so much of this project to their incredible teaching and mentorship. Not only them, but I am thankful for all the members of the CASPER research group who taught me and worked with me for the past few years: Dr. Katie Vermillion, Dr. Eva Kostadinova; the graduate students Graeson Griffin, Calvin Carmichael, Parker Adamson, and Alexandria Mendoza; and my peers Jorge Martinez, Emerson Gehr, and Rahul Banka. Thank you to Jessica Friberg, my writing buddy, for moral support as well as commiseration. Thank you to Matt Young, for encouraging and supporting me. And thank you to my family, for always believing in me.

Support for this work from NSF grant numbers 1903450 and 1740203, NASA grant number 1571701, and the U.S. Department of Energy, Office of Science, Office of Fusion Energy Sciences under award number DE-SC-0021334.

I gratefully acknowledge the joint ESA - Roscosmos "Experiment Plasmakristall-4" onboard the International Space Station. The microgravity research is funded by the space administration of the Deutsches Zentrum für Luft- und Raumfahrt eV with funds from the federal ministry for economy and technology according to a resolution of the Deutscher Bundestag under Grants No. 50WM1441 and No. 50WM2044.

CHAPTER ONE

1 An Introduction to Complex Plasmas

1.1 History of Dusty Plasma

1.1.1 What is a Plasma?

My quick Google search of the word "plasma" yielded about 835,000,000 results in 0.56 seconds, with the first few hits referring to the most commonly known definition of plasma: the liquid part of blood that makes up about 55% of blood's overall content ("What Is Plasma? - Health Encyclopedia - University of Rochester Medical Center" n.d.). However, continuing to read down the list of results reveals a different definition of the word. In physics, plasma is an ionized gas: a distinct state of matter consisting of charged ions and electrons in a gaseous state. It is easy to visualize the phase transitions from solid to liquid to gas because we utilize them every day: leave an ice cube out at room temperature, and it melts into water. Boil water on the stove, and it evaporates into water vapor. Each of these transitions occurs as thermal energy is added to the system. Similarly, it is adding energy to a gaseous system that causes the ionization of gas, generating the fourth stage of matter: plasma.

In our daily lives, we are rarely aware of watching the phase transition from a gas to a plasma because the everyday occurrences of plasmas are often rare and sudden: lightning, flames, the Northern lights, and neon signs. We do not often think of these flashes of light as a state of matter, and encounters with solids, liquids, and gases are far more common. However, beyond the confines of Earth's atmosphere, plasmas are ubiquitous in the form of our own Sun, other stars, and a large portion of the interstellar and intergalactic medium, making up 99% of matter in the visible universe (Gurnett and Bhattacharjee 2017).

Normal matter – by which I mean a solid, liquid, or gas – is made of atoms, and all atoms are made of up a dense, positively charged nucleus and a number of negatively charged electrons that are bound to that nucleus. In typical solids, liquids, and gases, the charge in the nucleus is equal and opposite to that of the electrons, so that the overall electric charge on an atom is neutral. A plasma is generated when enough energy is added to an atom in a gaseous state that one or more electrons are pulled from the atom, changing an ordinary gas into a gas of neutral atoms, positive ions, and negative electrons. In laboratory experiments, this is often achieved by applying a strong electric field, polarizing the cloud of electrons around the nucleus of the atom and inducing a dipole, as shown in Figure 1. As the positive nucleus and the negative electrons are forced in opposite directions by the applied electric field, a sufficiently strong field which supplies energy beyond the atom's ionization energy will strip individual electrons from their constituent atoms, forming a gaseous system of freely moving ions and electrons.

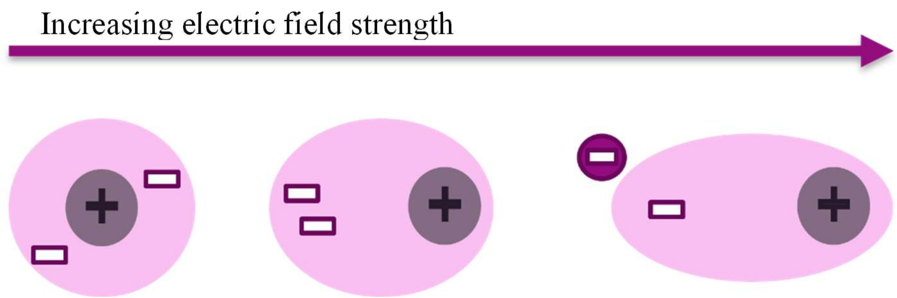

Figure 1: Polarization of a neutral gas atom by applying a strong electric field leads to ionization, generating a plasma. The leftmost image indicates a neutral atom in the absence of an electric field. The central image is a polarized atom, and the image on the right shows an ionized atom, where an electron is no longer bound to the atom.

The focus of this thesis is on complex, or dusty, plasmas, which consist of solid microparticles suspended in an ionized gas. The presence of these microparticles, which are often called dust, alters the dynamics of the plasma, creating a complex system that is useful for studying a range of topics from the formation of planets to the self-organization of atoms in normal matter.

1.1.2 Beginnings of Plasma Science

The first description of a complex plasma may have been made by Irving Langmuir in 1924, even before he coined the term "plasma" to describe ionized gases. In his paper, "A New Type of Electric Discharge: The Streamer Discharge," Langmuir describes his experimental setup, which involves an argon discharge – a plasma generated by ionizing argon gas between two electrodes – and a ring of solid tungsten in a glass bulb.

> … the tube is filled with extremely pure argon gas at a pressure of preferably 2 to 4 mm of Hg. The cathode is heated to about 2500° K and +250 volts is applied to the anode through a resistance. By approaching one terminal of a high frequency coil to the middle of the glass tube an arc of about one ampere is started though the tube, and the voltage difference between anode and cathode falls to about 25

> volts. The arc then fills the tube with a uniform pale reddish glow showing only lines of the red argon spectrum. (Langmuir, Found, and Dittmer 1924)

After creating the stable argon discharge, which would be classified as an ordinary (non-complex) plasma, Langmuir begins the process of starting the "streamer discharge" by sputtering droplets of tungsten into the argon plasma. By sputtering tungsten inside the bulb, the discharge is immediately changed as small, spherical tungsten droplets become suspended in the charged gas, and Langmuir observes one of the earliest occurrences of laboratory complex plasma. Langmuir first describes "brilliant blue flashes of light" as the tungsten vapor distributes throughout the discharge. The discharge seems to almost return to its original condition, but it exhibits translucent, golden skin and shows remarkable sensitivity to weak magnetic fields, as it is now easily deflected by a handheld horseshoe magnet.

Langmuir sees "little droplets of golden yellow liquid fire" form, break away from the skin, and drift into the arc of the discharge. He finds that he can manipulate the motion of the millimeter-sized droplets with magnets, and that as the droplets are guided along the axis of the discharge in either direction, they emit bright light.

> By regulating the intensity of the magnetic field these droplets, or globules, ranging from a few tenths mm up to 5 or 6 mm in diameter, can be made to form slowly and detach themselves singly from the skin of the arc. They usually move all the way across the arc and disappear when they reach the opposite boundary close to the glass wall. But by proper combinations of longitudinal and transverse fields the globules may often be made to move upwards or downwards in the arc parallel to its axis for distances of 5-10 cm. The light emitted by the globules is nearly white and is enormously more brilliant than that from the yellow skin of the arc. Under certain conditions the globules have been observed to move very slowly so that the motion through the arc could be easily followed by the unaided eye. But more often they move at velocities of 10 to 30 cm per second and thus appear as brilliant lines or filamentary streamers. (Langmuir, Found, and Dittmer 1924)

This experiment – the observation of small particles afloat within an ionized gas discharge that exhibit ordered motion along the axial direction – is a precursor to complex plasma experiments today. Langmuir's observations that the globules highly altered the discharge, making it more sensitive to external conditions such as the applied magnetic fields, and his remark that the globules could often be followed by the unaided eye are important realization that remain important to the study of complex plasmas. Complex plasmas have been shown to exhibit sensitivity to external fields in the manner of electrorheological fluids (Ivlev et al. 2008), and since they are easy to see, they are easy to study. Technically speaking, complex plasmas are "optically thin," meaning that they can be scanned and imaged quickly, easily, and non-destructively, making them an excellent model system for physical systems that are harder to observe.

Though the precise date that Langmuir actually coined the term "plasma" to describe the gas discharged he had been studying remains unknown, it was not until several years after his discovery of the streamer discharge, probably in 1927 or 1928. According to Lewi Tonks, who worked with Langmuir at the time, the story goes like this:

> Langmuir came into my room at the General Electronics Research Laboratory one day and said, "Say, Tonks, I'm looking for a word. In these gas discharges we call the region in the immediate neighborhood of the wall or an electrode a 'sheath,' and that seems to be quite appropriate; but what should we call the main part of the discharge? The conductivity is high so that you can't apply a potential difference to it like you can to a sheath. And there is complete space-charge neutralization. I don't want to invent a word, but it must be descriptive of this kind of a region as distinct from a sheath. What do you suggest?" (Tonks 1967)

Tonks provided the classic response – "I'll think about it" – but the next day, Langmuir had found the word he was looking for. "I know what we'll call it! We'll call it the 'plasma'" (Tonks 1967). Harold Mott-Smith, who was also working with Langmuir in the 1920s, recalls Langmuir's choice for the word in in connection to blood plasma, writing:

> He (Langmuir) pointed out that the "equilibrium" part of the discharge acted as a sort of sub-stratum carrying particles of special kinds, like high-velocity electrons from thermionic filaments, molecules and ions of gas impurities. This reminds him of the way blood plasma carries around red and white corpuscles and germs. So he proposed to call our "uniform discharge" a "plasma". Of course we all agreed. (Mott-Smith 1971)

Having given them a name, Langmuir and others continued to study plasmas and their fascinating behavior, and the field of plasma physics began to develop.

1.1.3 Influential Discoveries in the Field of Dusty Plasmas

Langmuir's early work in plasmas undoubtably influenced the birth of plasma science, but it was not until the 1980s that several watershed discoveries caused increased interest in the field of dusty plasmas, sparking an interdisciplinary collaboration that led to the birth of a new and distinct field in physics: complex or "dusty" plasmas (Merlino and Goree 2004).

The first of these discoveries came from images taken by *Voyager 2,* which encountered the Saturn system in November 1980. These images revealed the mysterious existence of "spokes" – the dark, axial streaks shown in Figure 2– in Saturn's B ring that were observed to form features covering 6000 km across the ring in time durations as short as 5 minutes (Smith et al. 1982). A theory was proposed for the formation of these spokes by Goertz and Morfill in 1983, and revisited by Morfill and Thomas in 2005, that these spokes could be generated by a dusty plasma phenomenon.

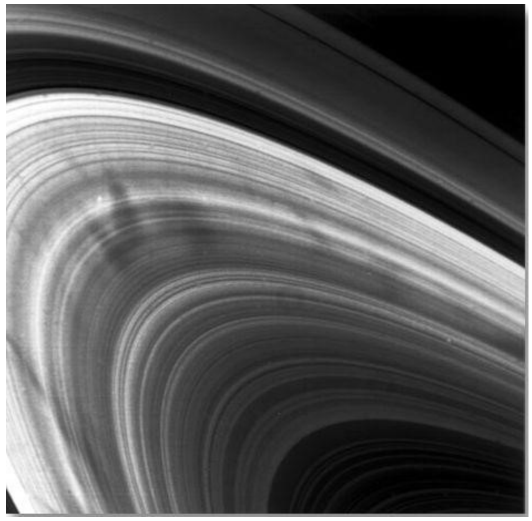

Figure 2: Photo of spokes in Saturn's B ring.
https://solarsystem.nasa.gov/resources/11501/ring-spokes/

Goertz and Morfill proposed that the formation of spokes in Saturn's rings would not be possible without a source of trapped plasma within the ring. The trapped plasma would contribute enough electron density to loft significant portions of dust, enough to explain the observed ring phenomenon, but it remained unknown how a significant amount of plasma could be formed within the ring.

It was shown that the photoelectron flux due to sunlight at certain inclination of the rings with respect to the Sun was not necessarily enough to explain the dust elevation; further, it had been observed that the formation of spokes seemed independent of whether the ring area was in sunlight or shadow (Smith et al. 1982). So, the Goertz and Morfill model proposed the impact of meteoroids on the rings as an additional source of neutral and ionized gas withing the ring, creating a dense plasma cloud that would drift axially along the rings, elevating dust along its path (Goertz and Morfill 1983; G. E. Morfill and

Thomas 2005). The physics of dusty plasmas triumphed in elucidating the mystery of spokes observed in Saturn's rings.

Meanwhile, in the totally unrelated field of semiconductor manufacturing, another mystery involving charged dust arose when IBM staff scientist Gary Selwyn discovered that the meticulous process of etching of silicon wafers was being mysteriously sabotaged by dust present in the system, in spite of clean-room regulations that had been effective in removing dust in the past. The year was 1989, and semiconductor technology was improving steadily according to the trend of Moore's Law, which predicted that the number of transistors on a microchip would double every two years – meaning that the size of transistor components was steadily growing smaller. Smaller circuit components meant that even tiny dust grains could be enough to destroy a microchip.

At the time, IBM was using beams of rf plasma to perform the detailed etching of the silicon wafers in rooms that were painstakingly kept clear of dust. However, chip after chip were found defective due to dust contamination. In his investigation, Selwyn determined that the dust removed from the wafer in the etching process could become trapped in the sheath region of the rf plasma. There, the dust would cluster and clump together until the power was switched off, at which point the particles would fall and contaminate the wafer, rendering it unusable. The dust in the clean room was being generated by the etching process itself, and the circuit components were so small that these trapped dust grains were enough to destroy the chips (Selwyn, Singh, and Bennett 1989).

Semiconductor manufacturing at IBM – a company that was producing the first personal computers – and the exploration and imaging of outer space: two exciting fields of the frontiers of science which appeared to have nothing in common until they both revealed a need to understand the behavior of charged dust in a plasma environment. Fueled by these events, the field of complex or "dusty" plasma began to grow (Merlino and Goree 2004). As "dusty plasmas" gained scientific renown, it became clear that a standardized method of studying complex plasmas in a controlled environment would be necessary to allow for replicable results.

1.1.4 The Modern Field of Complex Plasma Science

The field of complex plasmas was born out of interdisciplinary collaboration between scientific fields, and the spirit of collaboration continued into the adolescent years of the field. At the 1988 Gaseous Electronics Conference in Minneapolis, Minnesota, the efforts began to develop a "reference cell," that would provide researchers with a standardized experimental setup. By using the reference cell, independent researchers could make comparative measurements required to characterize the plasma conditions needed to aid in developing methods for improved etching of semiconductors. The resulting reference cell, shown in Figure 3, was compatible with the commercial hardware being used to produce microchips, so that research and industry could more easily collaborate towards productivity in improving microprocessor fabrication (Brake, Pender, and Fournier 1999).

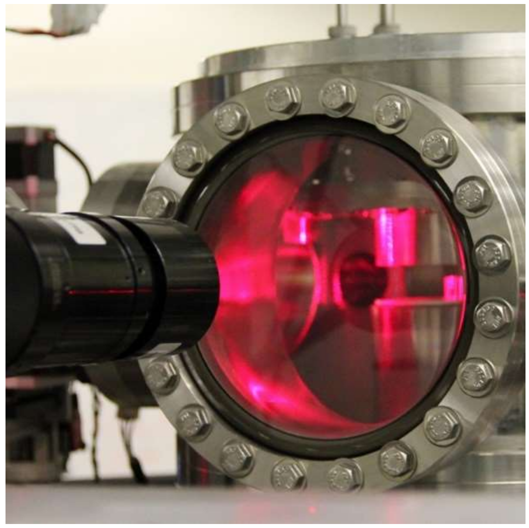

Figure 3: Plasma in a GEC reference cell at Baylor University. (Photo from https://www.baylor.edu/casper/)

While researchers in the semiconductor industry were preoccupied with removing the dust from their systems, investigators of astrophysical dusty plasmas were more interested in introducing dust into plasma experiments to understand the behavior of dust in these environments. In general, physicists were interested in the behavior of charged dust, as seen in the rings of Saturn and in the rf etching beams. As physicists began studying the details of dust motion in laboratory experiments, it became apparent that the dust acceleration was often dominated by a single force contribution – the force balance between the gravitational force and the electric force needed to loft a dust grain. For this reason, it became appealing to conduct complex plasma research in microgravity, where the strong electric fields necessary for experiments within Earth's gravitational pull were no longer required. The desire to carry out plasma research in space sparked another instance of collaboration between scientists, and a dusty plasma experiment became the first physics experiment to be conducted onboard the International Space Station (ISS). This experiment took place in the dusty plasma laboratory PKE-Nefedov, which was constructed on the ISS in order to study the long-term behavior of dusty plasmas in microgravity conditions (Nefedov et al. 2003).

1.2 Complex Plasmas as Soft Matter

Soft matter physics is a subdivision of the larger field of condensed matter physics and includes the study of materials that demonstrate macroscopic softness, such as granular solids or gels, and are sensitive to external equilibrium conditions (Morfill and Ivlev 2009). Morfill and Ivlev argue that complex plasmas may be understood as a state of soft matter and can also be used as a diagnostic system to understand the atomistic behavior of hard-to-study systems and phenomena such as active motion and phase transitions to metastable states.

In their 2009 review paper, Morfill and Ivlev emphasize the interdisciplinary nature of dusty plasmas, demonstrating that these systems provide ground for research in three primary areas. First, for the study of complex plasmas as a new state of soft matter, leading to investigations of the fundamental properties including wave propagation in complex plasmas and the phase diagram of dust in plasma. Second, the authors demonstrate that complex plasmas can be used to study the generic strong-coupling phenomena, drawing analogies to the strong coupling exhibited by complex liquids, regular liquids, and crystal structures. Finally, the authors direct the reader's attention to several possible application-oriented research opportunities related to dust mitigation in electronics manufacturing and tokamak fusion plasmas. Each of these topics provides motivation for the detailed study of the physics of complex plasmas, but particularly provides a framework for the possibility of using complex plasmas as an analogous system for non-plasma soft matter, such as the physics of biological systems on the microscopic scale.

1.2.1 Non-Hamiltonian Systems

One of the general properties of the soft-matter state of complex plasmas is that they are non-Hamiltonian, meaning they include a form of dissipation of energy that prevents them from being fully described by the standard energy operator. In many systems, the presence of friction makes them non-Hamiltonian; in complex plasmas, it is a combination of the friction between dust and neutral gas and the presence of the ion-wake (described in detail in Section 2.3) that introduces non-reciprocity to the system, making it non-Hamiltonian. It is this energy dissipation that allows for systems to exhibit bottom-up self-organization into structures with spatial or temporal stability; one such example is lane formation (Chakrabarti et al. 2004). Self-organization is an important quality for development of new nanotechnology and nanomaterials, and it is analogous to the self-assembly of biological systems and the functionality of DNA (Nardin and Schlaad 2021).

1.2.2 Dust Phases in Analogy to Atomistic Motion

Complex plasmas have been shown to exhibit several distinct dust phases, characterized by the coupling of dust-dust interactions between particles. The coupling strength is defined by the ratio of the electrostatic potential energy to the kinetic energy of the dust. In 1986 it was theorized that with sufficiently high coupling strength, crystalline structures could form, providing the theoretical prediction of a crystal phase for complex plasmas (Ikezi 1986). This prediction led to the eventual experimental realization of the so-called plasma crystal, a 2D configuration in which levitated dust forms a monolayer exhibiting well-defined crystalline structure (Hayashi and Tachibana 1994; Chu and I 1994; Thomas et al. 1994). The discovery of plasma crystals provides a model system for studying phase transitions to and from a crystal structure, which has been an interesting problem for physicists since the theory of the Wigner crystal in the 1930s (Thomas et al. 1994). The ordered structure of the plasma crystal parallels the inter-atomic spacing of atoms in a normal solid, where atoms are bound in a particular lattice structure. Unlike normal solids, plasma crystals are observable without cutting-edge microscopy techniques, and micron-sized dust can even be seen with the unaided eye if it is properly illuminated.

Plasma crystals can undergo similar phase transitions to normal solids: in response to changing plasma parameters such as pressure and power, crystals undergo melting and freezing. This does not mean that the dust particles themselves are melting or freezing. Rather, it means that the interparticle interactions between dust grains can transition from a strongly coupled, solid-like state to a "melted" state where dust particles move freely with respect to each other. The language of "melting" or "freezing" characterizes the interactions between dust grains. Because plasma crystals are optically thin and easy to image, the phase transition of a plasma crystal "melting" and "freezing" can be imaged directly, using a high-speed video camera, making the transition simple to study. Conclusions about the melting or freezing transition in plasma crystals can illuminate our understanding of analogous transitions in normal crystals.

Complex plasmas also exhibit liquidlike phases when the coupling between dust particles in the plasma is not strong enough to form a crystal, but the dust-dust particles still strongly interact with their nearest neighbors (Chu and I 1994; Khrapak et al. 1999). Plasma liquids have been shown to emerge in capacitively-coupled rf plasmas as well as in the positive column of DC discharge plasmas, and exhibit fluidlike properties including convection and viscosity (Vorona et al. 2007). Complex plasma liquids also exhibit properties similar to electrorheological (ER) fluids (Ivlev et al. 2008), and liquid crystals, both of which are systems that demonstrate sensitivity to applied outside fields. Typical ER fluids are colloidal suspensions of microparticles in a non-conducting fluid, where the two materials have different dielectric constants, and dipole interactions emerge in the system when the microparticles themselves are polarized.

ER plasmas differ from conventional ER fluids in that the dipole interactions are due to the formation of ion "wakes" near dust particles, which create effective dipoles in the dust-plus-wake pair. Additionally, the neutral gas density is much lower than the fluid density in conventional ER fluids, so damping characteristics are far less significant in the ER plasma. This weak damping provides justification for using dusty plasmas as a better model system for investigating interparticle interactions and new physics in ER systems. Just as plasma crystals can illuminate the underlying physics of phase transitions to and from a crystalline state in normal matter, the physics of plasma liquids can help illuminate the physics of normal liquids or liquid crystals and their phase transitions (Evdokiya G. Kostadinova et al. 2023).

1.3 Structure of Thesis

This thesis is largely motivated by the connection between complex plasma and the physics of soft matter systems, particularly the liquidlike structures that have been shown to form in microgravity plasma clouds in the PK-4 experiment. Chapter 2 of this thesis describes the underlying physics of complex plasmas, providing the necessary theoretical background for a computational investigation of the isotropic-to-string transition in a complex plasma. In Chapter 3, concepts of the previous chapter are integrated into DRIAD (Dynamic Response of Ions And Dust), a numerical model of dust and ions in plasma. The DRIAD simulation uses a combined Molecular Dynamics (MD) and Monte-Carlo-Collision (MCC) method to simulate the dynamics of individual ions and dust in the complex plasma. Chapter 4 shares simulation results of a large cloud of dust particles undergoing the phase transition to a liquid-like structure at two different pressures, 40 Pa and 60 Pa. The final, liquid-like phase is analyzed at both pressures using pair correlation functions in one, two, and three dimensions, as well as the bond orientational correlation $g_6(r)$. A brief concluding chapter reflects on the concept of analogous systems in physics, leaning on the philosophical framework outlined by philosopher of science Mary Hesse in her work *Models and Analogies in Science*. I will connect the physics of complex plasmas with the analogous systems of ER fluids, liquid crystals, and self-ordering in biological systems in order to demonstrate the creative interplay between dusty plasma research and application-oriented research, discussing future applications and new frontiers for complex plasma science.

CHAPTER 2

2 Physics of Dusty Plasmas

2.1 Defining a Plasma

2.1.1 Ionization and Quasi-neutrality

A plasma is called the fourth state of matter because, in the same way that adding heat to a liquid induces the phase transition from a liquid to a gas, a plasma is formed from a gas through the addition of energy, which leads to total or partial ionization of the originally neutral gas. To generate a plasma, an ionization source must generate enough energy to excite constituent gas atoms beyond their ionization energy, stripping electrons from neutral gas particles to create a quasi-neutral fluid of electrons and ions. In the laboratory, plasma may be generated by an electric field, which polarizes atoms and then strips the electrons away from their constituent atoms. Plasmas may also be generated by heating a gas to a high temperature or exposing it to very high energy photons through x-rays or ultraviolet light (Gurnett and Bhattacharjee 2017). This ionization process gives rise to the condition that

$$n_e \cong Z n_i \tag{2.1}$$

where n_e is the number density of electrons and n_i is the number density of ions and Z is the charge state of the ion. Because each electron is introduced to the plasma by removing it from a neutral atom, the density of free electrons corresponds to the density of ionized atoms, allowing us to impose the general expression of quasi-neutrality:

$$q_e n_e + q_i n_i = 0 \tag{2.2}$$

where q_e and q_i are the charge on an electron and an ion, respectively. Quasi-neutrality is a general characteristic of plasma, but localized deviations from this equilibrium are far from trivial and generate interesting physical phenomena as variations in electric potential can drive shielding effects that give rise to mechanisms of self-organization in plasma.

In addition to their initial ionization, laboratory plasmas must be maintained by a continual energy source in order to sustain the plasma state, otherwise, electrons and ions will simply recombine. Naturally occurring plasmas may be created for a very short period of time – picture a bolt of lightning – or in a sustained environment like a solar nebula. Once ionized, gas particles may recombine with their lost electrons, returning to a neutral gas state, so a sustained plasma requires that the collision frequency between ions and electrons must be low compared with the ion-neutral collision frequency. As thermal energy is transferred between particles though collisions, ions and neutral gas atoms reach a thermal equilibrium with each other, while electrons are continually energized by the applied electric field and remain at a higher temperature. The difference between ion and electron equilibrium temperatures remains significant. The low frequency of collisions between species prevents thermal equilibrium across the system from being reached quickly, classifying a plasma as a system far from thermodynamic equilibrium (Gurnett and Bhattacharjee 2017).

2.1.2 The Debye Length

In order to justify the claim that plasmas experience distinct differences in thermodynamic properties between constituent species, it is helpful to define characteristic length scales that describe the interactions between ions and electrons. Because ions (+) have the opposite charge of electrons (−), the plasma is net electrically neutral and functions as a conducting fluid, where the free movement of electrons in plasma is analogous to the electron sea present in a conductor. The mobility of charged particles allows the plasma to electrostatically shield local charge densities within the bulk of the plasma. The primary length scale relevant to plasma physics is the Debye length, which describes the length at which electrons shield the charge of a positive test charge in plasma, a phenomenon known as Debye shielding. The Debye length is named for the Dutch physicist Peter Debye, who is credited with formulating the concept in its original form.

Imagine introducing a positive test charge into the plasma environment. Very quickly, negatively charged electrons will move close to the test charge because of the Coulomb force, while positive ions will move away from the area surrounding the positive test charge, creating a cloud of net negative potential close to the test charge, shielding the positive charge a certain distance away.

The characteristic length of this shielding effect can be derived from modeling the electrons in the plasma statistically. Electrons are assumed to be distributed according to a one-dimensional Maxwellian (Melzer 2019)

$$f_s(v) = A\, e^{-\frac{\frac{1}{2}mv^2}{k_B T}} \tag{2.3}$$

where the distribution is given as a function of the electron velocity, v. Here, m is the mass of the particle species in kg, k_B is Boltzmann's constant, and T is the temperature in Kelvin. This is a velocity distribution in 1-dimensional velocity space, where normalization constant, A, may be determined by imposing the normalization condition, which requires that the distribution integrated over all velocity space yields the particle density:

$$n_s = \int_{-\infty}^{\infty} f(v)dv \tag{2.4}$$

$$n_s = \int_{-\infty}^{\infty} Ae^{-\frac{mv^2}{2k_BT}} dv$$

$$n_s = A\sqrt{\frac{2\pi k_B T}{m}}$$

solving for A,

$$A = n_s\sqrt{\frac{m_s}{2\pi k_B T}}$$

This was carried out for one-dimensionally distributed data, but can be easily extended to fit the three-dimensional plasma environment (Gurnett and Bhattacharjee 2017). Under the assumption of isotropic particle velocities, and allowing the energy term to carry an additional potential energy term, the distribution becomes

$$f_s(v) = n_0\left(\frac{m_s}{2\pi k_B T}\right)^{\frac{3}{2}} e^{-(m_s v^2 - 2e\Phi)/2k_BT}$$

where n_0 is the background density of the electrons, which is can be set equal to the number density of electrons in a singly-ionized and quasi-neutral plasma.

In the presence of a non-zero electric potential, the energy term in the distribution function must be modified to include the electric potential energy, $-e\phi$, where e is the magnitude of the electron charge. The three-dimensional Maxwellian may be integrated in three-dimensional velocity space to yield the electron number density:

$$n_e = \int_{-\infty}^{\infty} n_0 \left(\frac{m_s}{2\pi k_B T}\right)^{\frac{3}{2}} e^{-\frac{(m_s v^2 - 2e\Phi)}{2k_B T}} v^2 dv \iint \cos(\theta)\, d\Omega \tag{2.5}$$

$$= 4\pi n_0 \left(\frac{m_s}{2\pi k_B T}\right)^{\frac{3}{2}} e^{\frac{e\Phi}{k_B T}} \sqrt{2\pi} \left(\frac{k_B T}{m_s}\right)^{\frac{3}{2}}$$

$$n_e = n_0 e^{\frac{e\phi}{k_B T}} \tag{2.6}$$

where $n_0$is the background density of the electrons, which can be taken to be equal to the number density of the ions n_i in s singly-ionized quasi-neutral plasma, k_B is Boltzmann's constant, e is the charge on an electron, ϕ is the electric potential, and T is the temperature in Kelvin. The electric potential, ϕ, may be found from Maxwell's equation relating the electric field $\vec{E}$ to the charge density ρ:

$$\nabla \cdot \vec{E} = -\frac{\rho}{\epsilon_0} \tag{2.7}$$

where $\epsilon_0$is the permittivity of free space. The electric field can be expressed in terms of the electrostatic potential as

$$\vec{E} = -\nabla\phi \tag{2.8}$$

Substituting the potential form of the electric field back into Maxwell's equations, we arrive at Poisson's equation:

$$\nabla^2\phi = \frac{\rho}{\epsilon_0} \tag{2.9}$$

The volume charge density ρ in a given region is given by the assumption that ions are singly ionized, meaning that they carry a net positive charge of e, so

$$\rho = e\,(n_i - n_e) \tag{2.10}$$

where the local charge densities define the background potential at the particular point. Substituting this charge density into Poisson's equation,

$$\nabla^2\phi = \frac{\rho}{\epsilon_0} = \frac{e}{\epsilon_o}\,(n_i - n_e) \tag{2.11}$$

And using Eq. 2.6, we arrive at

$$\nabla^2\phi = \frac{e}{\epsilon_o}\,(n_i - n_e) = \frac{e}{\epsilon_0} n_i\left(1 - e^{\frac{e\phi}{k_B T}}\right) \tag{2.12}$$

Now, by expanding the exponential term in this expression as a Taylor series using

$$e^x \approx 1 + x - \frac{x^2}{2!} + \cdots \tag{2.13}$$

$$\epsilon_0\nabla^2\phi = \epsilon_0\frac{d^2}{dr^2}(r\phi) = en_i\left[\frac{e\phi}{k_B T_e} + \frac{1}{2}\left(\frac{e\phi}{k_B T_e}\right)^2 + \cdots\right] \tag{2.14}$$

Then, keeping only the linear term,

$$\epsilon_0\nabla^2\phi = \frac{n_i e^2}{k_B T_e}\phi \tag{2.15}$$

We can write the relevant terms of the Laplacian in spherical coordinates, treating the plasma as isotropic:

$$\nabla^2\phi = \frac{d^2}{dr^2}(r\phi) = \frac{n_i e^2}{\epsilon_0 k_B T_e}(r\phi) \tag{2.16}$$

and let the coefficient be defined as some constant factor, λ^2 (Gurnett and Bhattacharjee 2017). The general solution to this differential equation is given by

$$\phi = \frac{A}{r} e^{-r/\lambda_{\mathrm{D}}} \tag{2.17}$$

Where A is a constant and the Debye length, λ_D, is defined to be

$$\lambda_D \equiv \left(\frac{\epsilon_0 k_B T_e}{n_i e^2}\right)^{1/2} \tag{2.18}$$

where ϵ_0 is the permittivity of free space. The constant, $A = \frac{1}{4\pi\epsilon_0}Q$, is chosen to satisfy the condition that as r goes to zero, the potential will be given as a Coulomb potential, which characterizes a point charge, so the final solution is

$$\phi = \frac{1}{4\pi\epsilon_0}\frac{Q}{r}e^{-r/\lambda_D} \tag{2.19}$$

which is known as the Debye-Hückel (or Yukawa) potential.

The exponential factor in the Debye-Hückel potential causes the potential to decay more rapidly than the Coulomb potential, falling off by a factor of $e = 2.71828$ at a distance of one Debye length. In general, increasing the plasma density decreases the characteristic shielding length, as does decreasing the temperature of the electrons. It is often practical to express the Debye length in terms of the measurable quantities T_e and n_i, so that $\lambda_D = 0.69\sqrt{\frac{T_e}{n_i}}$ cm, where T_e is in K and n_0 is in cm^{-3} (Chen 2016).

The Debye length characterizes the plasma system by quantifying the length scale over which local charge variations can differ from quasi-neutrality. When the positive test charge is introduced into the plasma system, it is shielded by surrounding particles so that far (several Debye lengths) away from the test charge, the effects of its presence on the potential of the system are not felt. In order for a system to meet the condition of quasi-neutrality and display collective plasma behavior, the size of the system, L, must satisfy the condition $\lambda_D \ll L$ so that the system as a whole is quasi-neutral, and strong divergences from neutrality are shielded out on the scale of the system (Chen 2016).

2.2 Complex Plasma

A complex or dusty plasma is created by the introduction of nanometer- to micrometer-sized particles into the plasma environment. Just as the introduction of a test charge alters the short-range interactions between plasma particles and introduces shielding effects, the introduction of dust alters the plasma system and must be treated carefully. A complex plasma, like a standard plasma, is an ionized gas that displays collective behavior as a conducting fluid, demonstrates shielding, and does not easily reach a thermal equilibrium between plasma species. A complex plasma includes the additional parameter n_d, the number density of dust. Hence, the quasi-neutrality condition is modified to account for the charge on the dust

$$q_e n_e + q_i n_i + Q_d n_d = 0. \tag{2.20}$$

The introduction of dust into the plasma environment disturbs the quasi-neutrality of the plasma fluid as negative charges are collected on the surface of dust grains (as explained in Section 2.2.1). Just as electrons shield a positive test charge, as described in the derivation of the Debye length, the ions now play a role in shielding the negative charge of the dust grains. For complex plasmas, the ion Debye length describes the shielding of dust grains by ions:

$$\lambda_{Di} \equiv \left(\frac{\epsilon_0 k_B T_i}{n_i e^2}\right)^{1/2} \tag{2.21}$$

where T_i is the kinetic temperature of ions in K. This shielding is analogous to the shielding of ions by electrons, an effect which is present in all plasmas, with or without dust.

2.2.1 Plasma Frequency

Displacements of particles from equilibrium positions cause a restoring force proportional to that displacement. The motion of plasma particle – electrons, ions, and dust – around their equilibrium positions can be approximated as a harmonic oscillator because of the proportionality of the restoring force to the displacement (Hooke's Law):

$$F = -k\Delta x \tag{2.22}$$

Consider a slab of plasma consisting of an equal number of electrons and ions. As the ions are much heavier than the electrons, they may be treated as stationary with respect to the electrons (Figure 4).

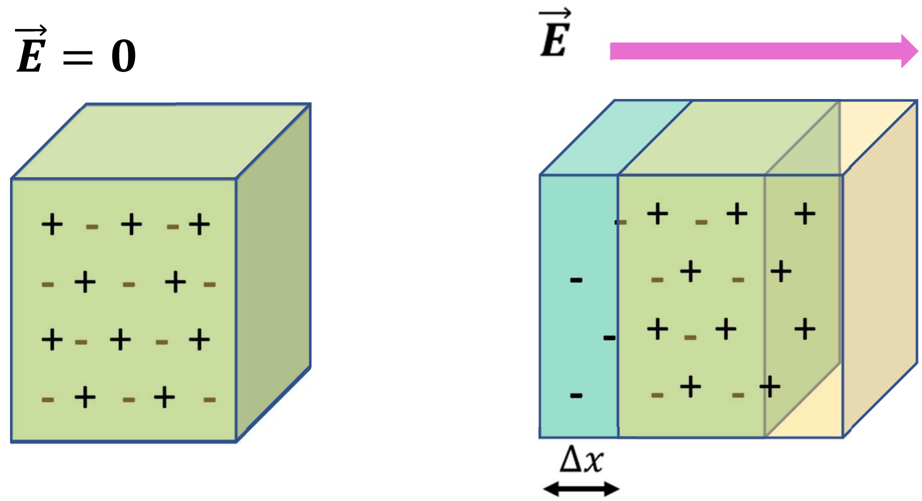

Figure 4: Schematic of a slab of plasma with no external field (left) and under the presence of an electric field (right).

If the electrons in the slab are displaced from equilibrium by a distance Δx, the electric field in the plasma in the Gaussian surface drawn in red in Figure 5 is given by Gauss's law:

$$\int \vec{E} \cdot d\vec{A} = \frac{Q_{enc}}{\epsilon_0} \tag{2.23}$$

$$\vec{E} lz = -\frac{en_e(\Delta x lz)}{\epsilon_0} \tag{2.24}$$

$$\vec{E} = -\frac{en_e \Delta x}{\epsilon_0} \tag{2.25}$$

where the negative sign indicates that the electron displacement, Δx, is in the opposite direction as the applied electric field.

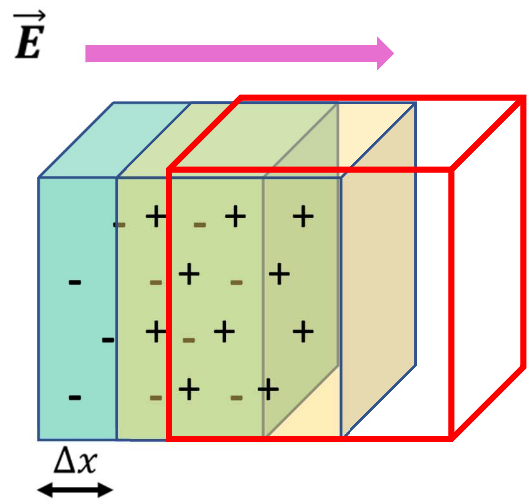

Figure 5: Schematic representation of the displacement associated with the plasma frequency, with the Gaussian surface shown in red.

The equation of motion when the electrons are released is given by

$$m\ddot{x} = \frac{d^2\Delta x}{dt^2} = -qE = -\frac{n_0 \mathrm{E}^2 \Delta x}{\epsilon_0} \tag{2.26}$$

Where q is the charge on an electron. This is simply the harmonic oscillator equation

$$\frac{d^2\Delta x}{dt^2} + \left(\frac{n_0 \mathrm{E}^2}{\epsilon_0}\right)\Delta x = 0 \tag{2.27}$$

The characteristic oscillation frequency is given by the term in parentheses, letting us define the electron plasma frequency as

$$\omega_{pe}^2 = \frac{n_0 e^2}{e_0 m_e} \tag{2.28}$$

Analogously defining a frequency for the displacement of ions,

$$\omega_{pi}^2 = \frac{n_0 e^2}{e_0 m_i} \tag{2.29}$$

it can be seen that $\omega_{pi} \ll \omega_{pe}$, because of the mass difference. As the timescale for the response of the particles is $\tau \propto \frac{1}{\omega}$, the time for ions to respond to a perturbing force is much greater than the time for electrons to respond to the same perturbing force. This will allow us to later make the simplification of assuming stationary ions when considering the motions of electrons, and stationary dust while considering ion motion, which is relevant to the model discussed in Chapter 3.

2.2.2 Dust Charging

It was asserted above that dust particles in a plasma acquire a negative charge, and thus exhibit shielding analogous to the shielding of ions by electrons. It is possible in certain plasma conditions for ions to be negatively charged rather than positively charged, and also possible for dust to acquire a positive charge instead of negative – such as in the case of an afterglow plasma (Chaubey and Goree 2022b). However, in the experimental and numerical conditions detailed in this paper, the assumptions required for negatively charged dust hold.

A conceptual understanding of why dust in plasma acquires a negative charge arises from the kinetic theory of gases, which gives the average velocity of particles as a function of temperature:

$$v_s = \sqrt{\frac{8k_B T_s}{\pi m_s}} \tag{2.30}$$

where the subscript denotes the particle species, either ion or electron. Even in thermal equilibrium, when $T_i = T_e$, the mass comparison $m_i \gg m_e$ causes $v_s > v_i$. Due to the greater mobility of electrons in plasma, a neutral object in the plasma environment will acquire a negative charge. Typically, laboratory plasmas will be far from thermodynamic equilibrium due to their low density; collisions between ions and electrons are infrequent, so they will approach thermal equilibrium quite slowly. However, collisions between ions and neutral gas particles occur frequently, so the ions reach thermal equilibrium with the neutral gas, which is usually at room temperature. In this case, $T_e > T_i$. The velocity comparison $v_e > v_i$ means that the initial electron flux to the dust surface will be greater than the ion flux, and the dust will initially charge negatively. As electrons are repelled from the negatively charged grain while ions are simultaneously attracted, the fluxes of the two species will change accordingly, which means that for some negative equilibrium dust charge, the electron and ion fluxes will be equal. Due to the greater mobility of electrons in plasma, a neutral object in the plasma environment will acquire a negative charge.

Accurate predictions of dust charge are commonly derived from the orbital motion limited (OML) theory, which is based on the principles of energy and momentum conservation. The first assumption of OML theory is that the condition that $a \ll \lambda_D \ll \lambda_f$, where a is the dust radius, λ_D is the electron Debye length, and λ_f is the mean free path of an electron or ion. This implies that the dust grains must be small and the plasma itself must have a low density in order for the OML theory to be applied.

The dust charge can be determined by considering the currents of charged particles to the dust surface. The general charging theory is based simply on conservation of energy and momentum by determining the collisional cross section of ions and electrons with the dust surface. To begin, we define an impact parameter b and critical value b_c, where particles with $b < b_c$ will collide with the dust grain and particles with $b > b_c$ will merely be deflected, as shown in Figure 6.

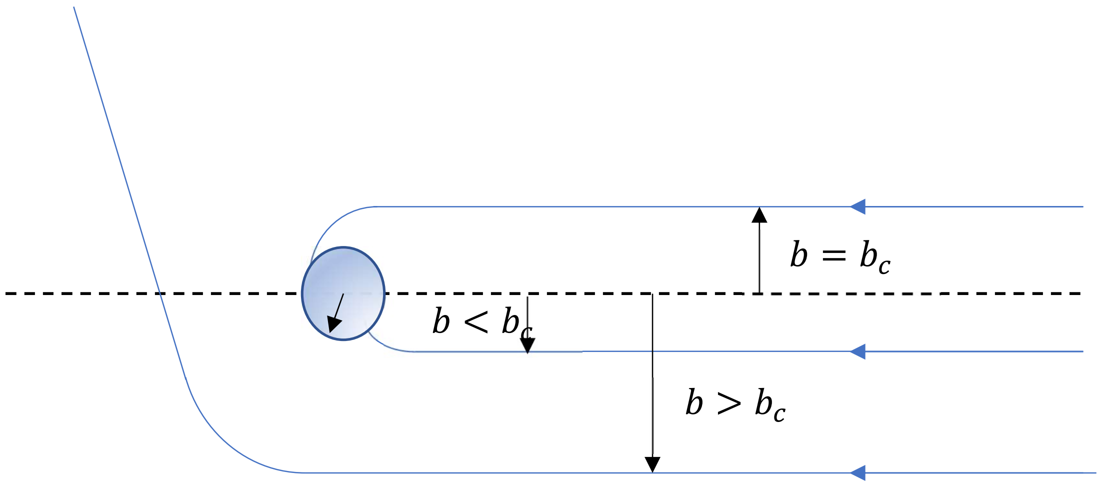

Figure 6: Diagram of impact parameters used in OML charging currents to dust grains.

Energy is conserved as ions approach the dust grain from infinity, where the electrostatic potential is taken to be zero:

$$\frac{1}{2}m_i v_{i,0}^2 = \frac{1}{2}m_i v_i^2 + e\Phi \tag{2.31}$$

Where m_i is the ion mass in kg, $v_{i,0}$ and v_i are the ion velocities far away and at the dust surface, respectively, in m/s, and Φ is the dust surface potential, which is considered to be negative. This may be rearranged to give

$$\frac{1}{2}m_i v_{i,0}^2 = \frac{1}{2}m_i v_{i,0}^2 \left(\frac{v_i^2}{v_{i,0}^2} + \frac{e\Phi}{\frac{1}{2}m_i v_{i,0}^2} \right) \tag{2.32}$$

The momentum of a particle with impact parameter b_c approaching from infinity is given by

$$L = |r \times b| = m_i v_{i,0} b_c \tag{2.33}$$

while the momentum of the particle impinging upon the surface is given by

$$L = m_i v_i a \tag{2.34}$$

Equating these quantities yields

$$m_i v_{i,0} b_c = L = m_i v_i a \tag{2.35}$$

$$m_i^2 v_{i,0}^2 b_c^2 = m_i^2 v_i^2 a^2 \tag{2.36}$$

$$\frac{v_i^2}{v_{i,0}^2} = \frac{b_c^2}{a^2} \tag{2.37}$$

which shows that the ratio of the dust radius squared $a^2$and the square of the impact parameter b_c^2 are proportional to the ratio of the velocities. Rewriting the right-hand side of Eq. 2.32 in terms of the impact parameter,

$$\frac{1}{2} m_i v_{i,0}^2 \left(\frac{v_i^2}{v_{i,0}^2} + \frac{e\Phi}{\frac{1}{2} m_i v_{i,0}^2} \right) = \frac{1}{2} m_i v_{i,0}^2 \left(\frac{b_c^2}{a^2} + \frac{e\Phi}{\frac{1}{2} m_i v_{i,0}^2} \right) \tag{2.38}$$

Where the dust radius squared a^2 and the impact parameter b_c^2 are proportional to the velocities. This yields the condition

$$\frac{b_c^2}{a^2} + \frac{e\Phi}{\frac{1}{2} m_i v_{i,0}^2} = 1 \tag{2.39}$$

so that the squared ion collection radius is given by

$$b_c^2 = a^2 (1 - \frac{2e\Phi}{m_i v_{i,0}^2}) \tag{2.40}$$

The geometric collisional cross section is given by

$$\sigma = \pi r^2 \tag{2.41}$$

where r is the radial distance from the center of a target that describes the distance for which incoming particles will be made to collide with the target. So, the cross section for ion collection is given by

$$\sigma_{c,i} = \pi a^2 (1 - \frac{2e\Phi}{m_i v_{i,0}^2}) \tag{2.42}$$

By analogy, the collision cross section for electrons is given by

$$\sigma_{c,e} = \pi a^2 (1 + \frac{2e\Phi}{m_e v_{e,0}^2}). \tag{2.43}$$

Since the potential Φ is understood to be a negative quantity, it is seen that the effective cross sections $\sigma_{c,i}$ and $\sigma_{c,e}$ are altered with respect to the actual collision cross section of the dust grain with radius a. $\sigma_{c,i}$ increases the collection radius of the dust, which makes sense because ions will be attractive to the negative potential of the dust grain. $\sigma_{c,i}$ effectively reduces the radius of the dust because of the repulsion between electrons and the dust surface.

The flux of electrons and ions to the dust surface may be integrated to obtain the electron and ion currents to the dust:

$$I_i = \pi a^2 n_i e \sqrt{\frac{(8k_B T_i)}{\pi m_i}} (1 - \frac{e\Phi}{k_B T_i}) \tag{2.44}$$

$$I_e = \pi a^2 n_e e \sqrt{\frac{(8k_B T_e)}{\pi m_i}} exp(-\frac{e\Phi}{k_B T_e}) \tag{2.45}$$

In equilibrium, the electron and ion currents are subject to the condition

$$I_i + I_e = \frac{dq}{dt} = 0 \tag{2.46}$$

By setting the negative electron current equal to the ion current, one obtains

$$I_i = \pi a^2 n_i e \sqrt{\frac{(8k_B T_i)}{\pi m_i}} \left(1 - \frac{e\Phi}{k_B T_i}\right) =$$

$$\pi a^2 n_e e \sqrt{\frac{(8k_B T_i)}{\pi m_i}} exp\left(\frac{e\Phi}{k_B T_i}\right) = I_e \tag{2.47}$$

Which can be analytically solved for the potential, Φ (Figure 7). For the case of a singly ionized hydrogen plasma when $T_e = T_i$, the numerical solution yields the classic result $\Phi = 2.51\frac{k_B T}{e}$ (Spitzer 1941)

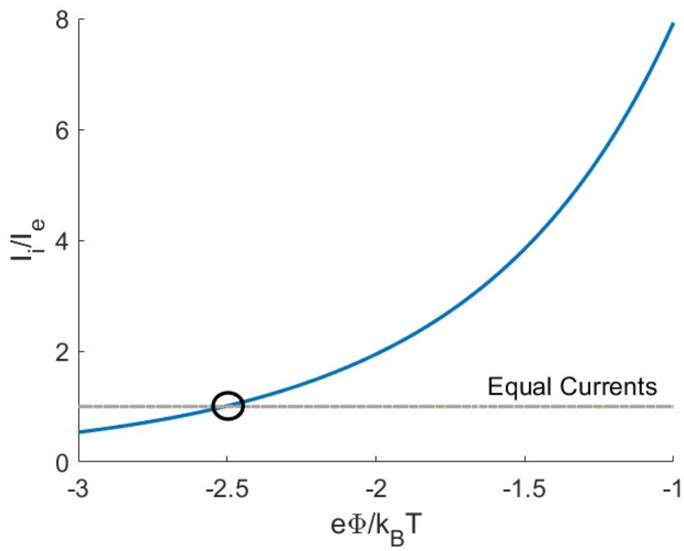

Figure 7: Analytic solution of electron and ion current balance from OML theory yields the result $\Phi = -2.51e/k_B T$. The equilibrium current is found when the ratio of ion and electron current equals one.

To find the charge on the dust grain from the floating potential, the dust grain can be approximated as a spherical capacitor. The capacitance of a sphere is typically given as $C_{spher} = 4\pi\epsilon_0 a$, where a is the radius. In a shielded plasma, the capacitance is altered: $C_{dust} = 4\pi\epsilon_0 a(1 + \frac{a}{\lambda_D})$, which reduces to the ordinary spherical case in the limit

$a \ll \lambda_D$, which we assume. The charge on a capacitor $Q = C\Phi$ is used to determine the dust charge as

$$Z_D = -4\pi\epsilon_0 a\Phi, \tag{2.48}$$

where Φ is the Debye-Hückel potential derived from the equilibrium condition in Equation 2.47.

2.3 The Ion Wake

Coulomb's law for charged objects tells us that the force between objects of opposite charge is attractive, while the force between like-charged objects is repulsive. So, when a negatively charged dust grain interacts with the plasma background, positive ions cluster around the dust grains in a shielding cloud. If there is a directional flow of the plasma fluid, it has been shown that the Debye shielding sphere is elongated along the direction of ion flow and displaced downstream of the dust grain, as shown in Figure 8. The region of ion concentration downstream of the dust grain is called the ion wake.

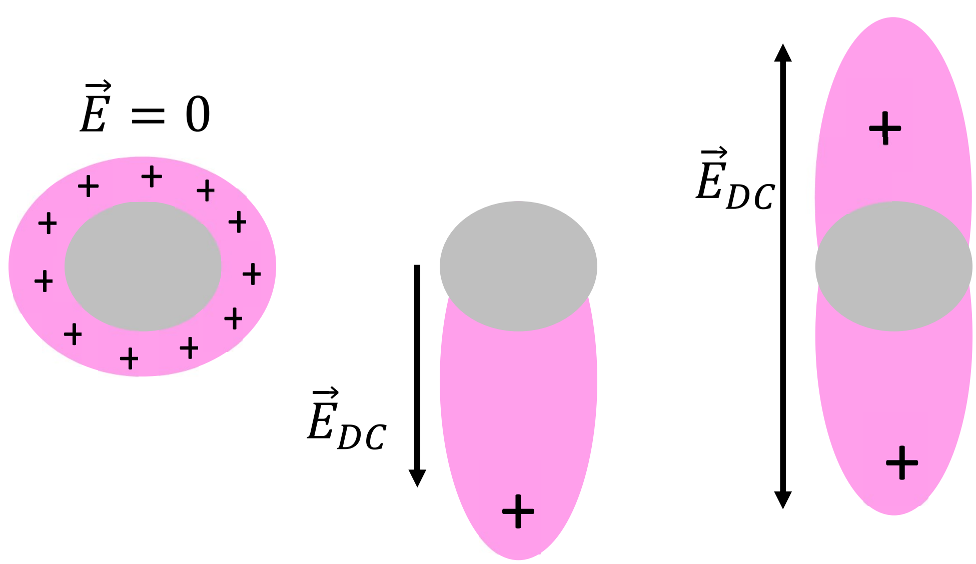

Figure 8: Diagram of the ion cloud in the vicinity of a negatively charged dust grain in the absence of an electric field (left), a DC electric field in one direction (center), and a polarity-switching DC electric field (right).

The positive space charge in the ion wake is thought to be responsible for the macroscopic self-organization exhibited by some plasma systems. As shown in Figure 9, the net attraction of a dust particle to a nearby particle is affected by the shielding ion cloud around the nearby particle. The ion background affects the reciprocity between dust-dust interactions because when grains align themselves along the direction of ion flow, the downstream grains experience stronger attraction to the upstream dust grain's wake than vice-versa.

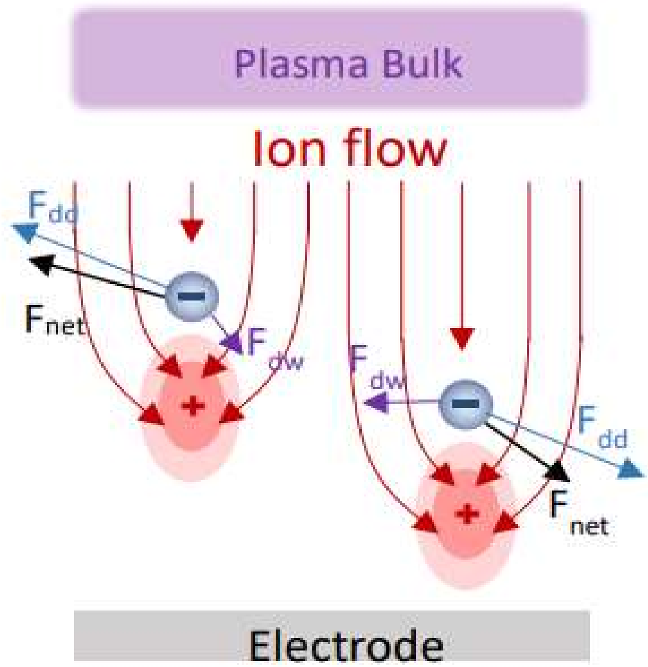

Figure 9: Diagram of the ion wake in flowing plasma. The force interaction between dust grains is reciprocal, as shown by the arrow $\mathrm{F_{dd}}$. The forces $\mathrm{F_{dw}}$ show the attraction between each dust grain and the other's ion wake, where the downstream grain is more strongly attracted to the upstream grain's wake than vice-versa. The net force between the two dust-wake systems is non-reciprocal, as shown by F_{ne} (Matthews 2020)

2.3.1 Non-Reciprocity

Newton's third law of motion, which states that for every action, there is an equal and opposite reaction, is one of the fundamental principles in classical physics. However, certain environments are said to be non-reciprocal, meaning they cannot be described by classical Hamiltonian dynamics, which assumes reciprocal interactions. A common example outside of plasma physics is the active motion of micro-swimmers in a chemical gradient. These swimmers draw energy from their surroundings, leading to diffusive motion that cannot be described with a Hamiltonian (Bechinger et al. 2016).

When microparticles are suspended in the plasma environment, the presence of an ion drift causes a concentration of ions downstream of the suspended microparticle called the ion wake. As charged particles act in the presence of ion flow, as discussed above, their interactions with the ion wake of neighboring particles are non-reciprocal because the ions act in a dynamic background (Ivlev et al. 2015). Though the force pair between dust particles remains reciprocal (F_{dd} in Figure. 9), the proximity between the charge center of the dust grain and the wake causes the difference between the magnitudes of the vectors F_{dw}. This leads the overall force between particles and their ion wakes (F_{net}) to break reciprocity, as the downstream particle is more strongly attracted to the upstream particle than vice versa (Matthews et al. 2020).

In a flowing plasma, the presence of the ion wake allows for non-reciprocal interaction between microparticles, which, in addition to confining forces, contributes to the stability of structures in the plasma environment. Wake-mediated interactions have been shown to give rise to electrorheological effects (Ivlev et al. 2008), where the plasma system demonstrates sensitivity to electric fields, self-organizing into a liquid-like structure, with chains of dust grains along the direction of an externally applied electric field (Evdokiya G. Kostadinova et al. 2023). These have been studied in detail through the Plasma-Kristall-4 (PK4) experiment onboard the International Space Station (ISS), as well as through numerical modeling (Vermillion et al. 2022).

CHAPTER 3

3 Experiments and Simulations: Modeling the PK4 with the DRIAD Simulation

3.1 The Connection between Experimental Results and Numerical Models

3.1.1 Merits of Modeling

When dusty plasmas are studied in the laboratory, observations are often corroborated by numerical models that display the same results. The agreement between numerical model and experiment is evidence of a valid conclusion; disagreement signifies a discrepancy between theory and reality. Numerical models work in an opposite direction than experiment because they draw simulated observations from mathematical theory, while experimental results are based directly on observation of an experiment and analysis of that observation. In simpler terms, modeling takes the abstract concepts – known physics equations – and uses them to create a picture that accurately reflects the experimental reality.

In complex plasma experiments, it is the recursive process between laboratory investigations and numerical modeling that leads to conclusive results about the underlying physics at play in the system. The aphorism "all models are wrong; some models are useful" is true for numerical physics, but studying physics is about artfully reducing the complexity of physical reality into formalizations that can be handled mathematically and computationally without causing too great a divergence from reality. "All models are wrong," but the appropriate simplifications often lead to the most illuminating conclusions. The results derived from numerical investigations – provided they do not contradict physical observations – are valid and extremely useful in the understanding of complicated systems. It is important to note that numerical results cannot validate themselves because they must be replicated experimentally to demonstrate that the result is physical, not simply an artifact of the inherent simplifications utilized by the model. Studying dusty plasmas experimentally and numerically focuses on this recursive process between a particular experiment and a corresponding numerical model. In this case, the numerical model DRIAD (Dynamic Response of Ions and Dust) was designed to investigate the behavior of complex plasmas in two experiments: the Plasma Kristall-4 (PK-4) and the GEC reference cell, which was mentioned in Chapter 1.

3.1.2 The PK-4

In this work, the DRIAD simulation is used to explicitly model the ions and dust in an environment based on the Plasma Kristall-4 (PK4), the fourth generation of a dusty plasma experiment on the International Space Station (Pustylnik et al. 2016). A diagram of the experiment is shown in Figure 10.

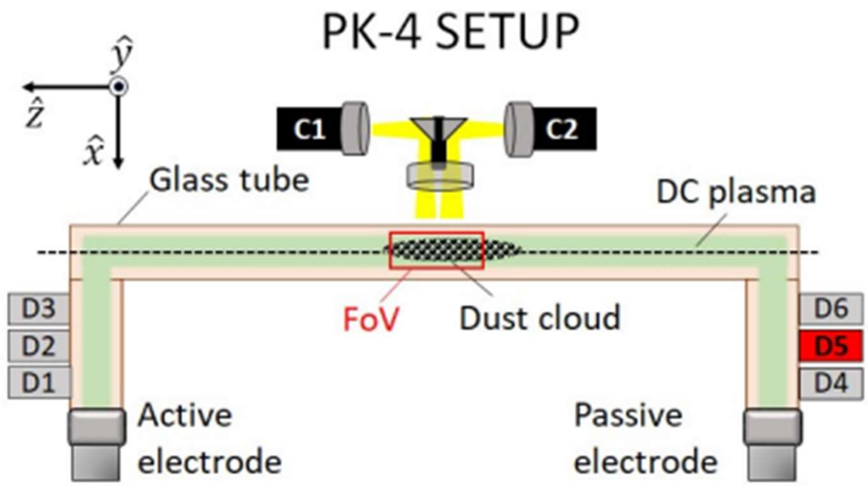

Figure 10: Schematic of the PK-4 onboard the ISS. (Vermillion et. al 2022)

Though dusty plasma experiments may be conducted on the ground, the benefit of conducting experiments in space is that strong electric fields needed to levitate the dust on Earth are no longer required in microgravity systems. This allows for finer tuning of the electric fields needed to maintain the plasma and allows experiments to reveal more about the interactions between the dust and ions in the plasma environment. On the ground, there is a lower limit placed on the strength of the electric field, because it must be large enough to balance the downward gravitational force. Hence, the microgravity conditions on the ISS are ideal for investigating the finely tuned interactions between the dust particles in the plasma as they self-organize into three-dimensional structures, analogous to classical solids and liquids, through their interaction with the plasma medium.

Microgravity conditions are ideal for investigating interesting complex plasma phenomenon that occur in 3D. Phase changes in plasma occur, in analogy to classical phase changes, when the interparticle interactions go from weakly interacting in the gaseous or liquid state, to strongly interacting, as in a classical solid. The "phase transitions" as a complex plasma becomes more ordered (freezing) or less ordered (melting) reveal information about the underlying physics behind phase transitions in true solids and liquids, so this is a fruitful and practical avenue for dusty plasma research. The microgravity conditions also allow for the study of fluid behavior such as shear flows (Nosenko et al. 2020) and electrorheology (Dietz et al. 2021).

The PK-4 laboratory consists of a Π-shaped vacuum chamber. The DC electric field that arises in the discharge plasma is used to trap levitated dust in the field of view of cameras in the center of the tube by alternating the polarity of the cathode and anode at a frequency that is high enough that the dust is not able to respond to the electric field. However, the lighter electrons can respond to the electric field and flow past the stationary dust grains. In this setup, the alternating direction of the DC field causes an elongation of the Debye shielding cloud, depicted in Figure11, stretching it in the direction of the field while dust particles remain relatively fixed in place.

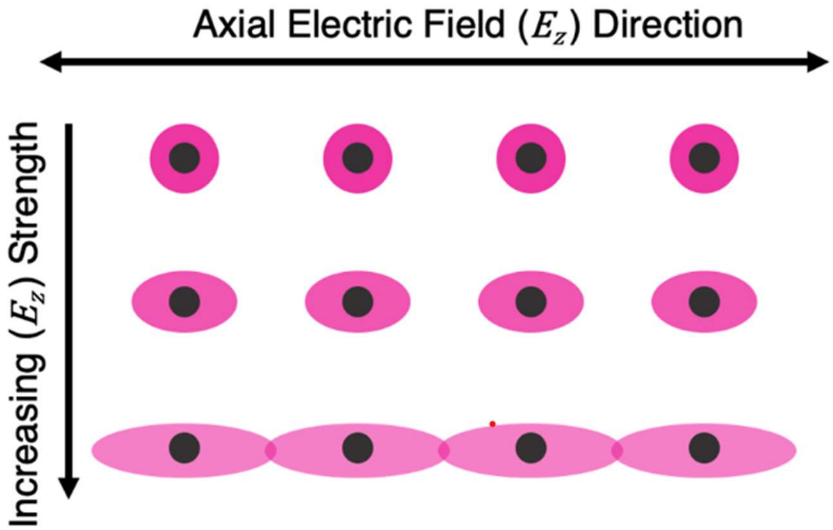

Figure 11: Wake elongation is dependent on applied electric field strength, and the rodlike dust-plus-wake system is analogous to elongated LC particles (Figure from Vermillion 2022).

This experiment is ideal for studying the transition from disordered, gas-like structure to liquidlike order in complex plasmas. Treating the dust grain along with its elongated ion wake as an analog to the liquid crystal (LC) particles is useful for analogously studying liquid crystal phase transitions (Evdokiya G. Kostadinova et al. 2023). The dust-plus-wake system is similar to rodlike LC particles that can become polarized and align with external electric fields according to the electrorheological effect.

In the experimental setup reflected in this numerical study, the PK4 uses a DC plasma with a frequency switching applied at 500 Hz. This polarity switching causes the ion drift to rapidly charge directions on a timescale that is fast enough that the dust particles do not react to the polarity switch and are thus trapped in the field of view of the used for imaging the dust throughout the experiment. From the experiment, the positions of the dust particles, recorded on video, can be used to obtain particle velocities through particle tracking. The position and velocity data are used to analyze the complex structures of the dust systems. This analysis can be compared with simulation data.

3.2 The DRIAD Simulation

3.2.1 General Information

The computational portion of this thesis utilizes the existing N-body simulation, DRIAD (Dynamic Response of Ions And Dust), that simulates the motion of both ions and dust particles in the plasma environment on their respective timescales (Lorin Swint Matthews et al. 2020). The DRIAD model is versatile and can be used to simulate a broad range of plasma environments and multiple coordinate systems, with or without the effects of gravity. This versatility allows the same base model to provide useful numerical data related to experiments in the rf plasma of a ground-based GEC cell or a DC plasma, accept time-evolving conditions for the background plasma environment, and utilize flexible boundary conditions that can be tailored to different types of confinement. The type of confinement can allow for the formation of vertical chains against gravity in the plasma sheath of an earth-based GEC cell (Ashrafi et al. 2020) or the formation of long strings in the plasma bulk of a microgravity environment (Vermillion et al. 2022; L. S. Matthews et al. 2021a).

DRIAD uses an asymmetric approach to model the interactions between the ions and the dust, inspired by Piel's MAD (Molecular Asymmetric Dynamics) code (Piel 2017), Ion-ion interactions are regulated by a Debye-Hückle (or Yukawa) potential to account for the shielding of the ions by electrons, while the force of the dust on the ions is derived from the unshielded Coulomb potential, as the electrons are depleted in the vicinity of the dust grains (Piel 2017). However, the force of the ions on the dust is derived from a

Debye-Hückle (Yukawa) potential. Piel's asymmetric approach chooses to sacrifice accuracy in the shielding of electrons while accounting for the non-linear shielding of dust grains by ions (Piel 2017). Though electrons are assumed to be Boltzmann distributed and are not simulated directly, the electrons are represented in the code not only in their contributions to the dust charge through OML theory, but also in the shielding term for the ion-ion and ion-dust interactions. The non-linear interactions between dust grains introduced by the ion-wake, which can allow for effective attractive forces between dust grains, are difficult to calculate. DRIAD models the motion of the ions in the vicinity of the charged dust grain, allowing the enhanced ion density to be examined in detail. The dynamic simulation allows the ion wake to charge as dust grains approach each other, and also self-consistently adjusts the charge on grains as they move within the wake of another grain. Piel's asymmetric approach chooses to sacrifice accuracy in the shielding of electrons while accounting for the non-linear shielding of dust grains by ions (Piel 2017).

3.2.2 N-Body versus Particle-In-Cell Methods

In general, there are several common models that have been used to study dusty plasmas, each with different associated computational advantages and disadvantages. The two primary models utilized are the Particle-In-Cell (PIC) method and the Molecular Dynamics (MD) method. DRIAD utilizes the latter approach, but because of the well-accepted use of the Particle-in-Cell method, this decision is worth justifying. The Particle-In-Cell, or PIC, approach is common method that uses fixed grid points to discretize equations by only solving the relevant physics at particular coordinates in space. Discretizing the fundamental physics equations remains true to the macro-level properties of the system without resorting to the simplifications of the molecular dynamics approach which require simplifications (e.g., not modeling electrons directly) due to their increased computational complexity. The PIC approach (Figure 12) is a good method to study complex, many-body systems, because computational time is controlled by the number of grid points used in the simulation. The computational complexity for PIC codes scales as $N + N_g \ln(N_g)$, where N_g is the number of grid points used in the simulation, compared with the N-body simulation that has complexity scaling by N^2 (Ludwig et al. 2012).

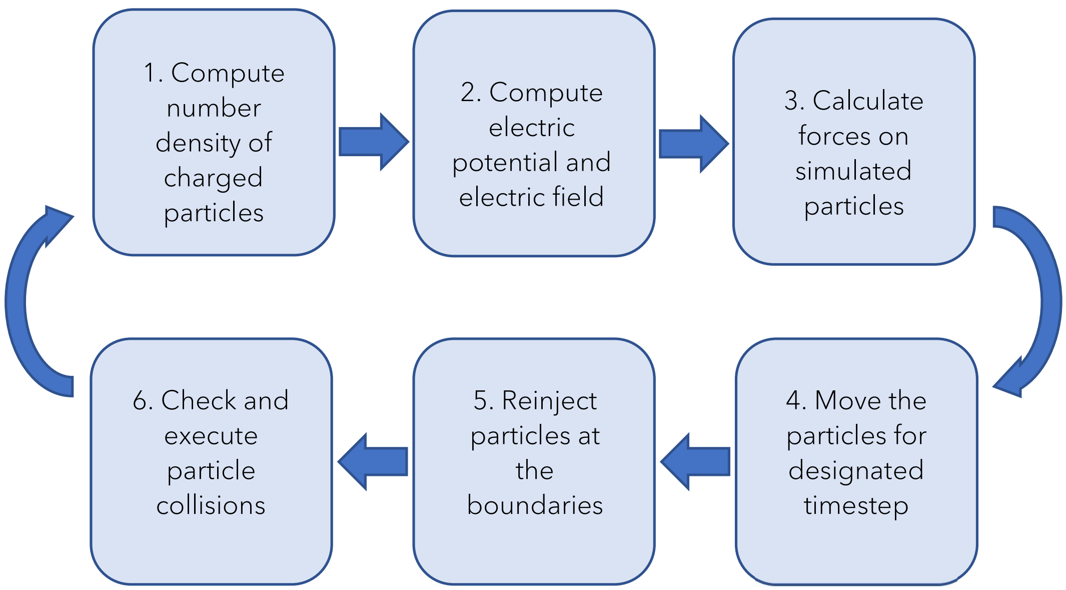

Figure 12: Basic steps of the PIC-MCC cycle (Donko 2021).

The number of grid points in a PIC code can be easily increased or decreased as needed, balancing the tradeoff between computation time and resolution. Complex grid refinements may also be used in cases when different resolution scales are needed to accurately represent the relevant data at different points in space. In the case of studying dusty plasmas, much greater resolution is needed for the areas close to dust grains, when the fine structure of shielding ion clouds is relevant to determining the resulting dust behavior. For this reason, it is often better to utilize a different algorithm to study dust in plasmas.

The common alternative to PIC codes is the N-body or Molecular Dynamics (MD) simulation, which calculates the force exerted on each dust particle by every other particle in the simulation at the-location of the particular particle in the simulation. This is computationally expensive, because calculations between interacting particles scale as N^2, making it difficult to simulate large numbers of particles. However, this method implicitly refines the grid to match the density of particles; calculations are performed for every particle, mitigating the risk of artificially smoothing data in areas of high particle density associated with PIC codes. Because of the MD approach's ability to account for the interaction of particles on a dynamic range of scales, it is a good approach for the dusty plasma system.

Because of the high number of particles in dusty plasma experiments, it is often reasonable to randomize certain aspects of the code, specifically the ion-neutral collisions, because the neutral gas particles are not modeled directly in the simulation. The DRIAD model utilizes the Monte Carlo Collision (MCC) method to randomize collisions between particles. For each timestep present in the simulation, a fixed number of collisions between simulated particles are chosen to collide, but the individual particle collisions are chosen randomly by the Monte Carlo method, effectively avoiding the possibility of artificially controlling collisions in some other way.

3.2.3 Utilizing the GPU Construction

The computational expense and long run times associated with MD simulations have been greatly improved through parallelizing the code by using the CUDA extension to the C programing language. GPU computing is useful for simulating the interactions between many bodies because simple calculations (e.g., the Coulomb force between every ion-dust pair in the simulation) can be carried out simultaneously rather than sequentially. DRIAD takes advantage of the speedup from GPU processing by using a combination of C++ and CUDA code. While the bulk of the DRIAD program is written in C++, the heart of the program - solving the individual particle equations of motions to determine the dynamics of ion and dust - is written in CUDA, so that the most time-consuming calculations are computed in parallel.

3.3 Implementing Plasma Physics

3.3.1 Dynamic Timescales

The complex plasma environment consists of electrons, ions, neutral gas, and dust particles. The DRIAD simulation models the ions and dust directly, and treats these two populations distinctly, solving the equations of motion for ions and dust on their respective timescales. Because the self-organization of microparticles in plasmas is largely due to the ion-wake effect, this consideration of independent timescales is vital for producing organized structures in the simulated dust cloud while remaining true to what happens physically. The ion timestep is typically set at 10^{-8} seconds, while the dust timestep is usually set at 10^{-4} seconds; these time resolutions may be diminished in some cases to decrease computational time, but the resolution must be enough that the ions equilibrate in their timescale before the dust particles are allowed to move in response. Likewise, time evolving plasma conditions reflect the rapid fluctuations in the background plasma – ion and electron density, temperature, ion drift velocity, and electric field – that are seen in the experiment (Hartmann et al. 2020). We typically allow 100 – 200 ion timesteps to cover an ion plasma period, usually about 1 microsecond, which insures that ions are able to equilibrate with the background plasma before moving the dust.

3.3.2 Treatment of Electrons and Neutral Gas

Electrons and neutral gas are important to the plasma environment, but need not be simulated directly in the DRIAD model. As discussed above, the electrons are present implicitly in the charging of the dust grains and the shielding term in the Yukawa potential that governs ion-ion interactions. Similarly, the presence of neutral (un-ionized) gas molecules are not modeled directly, but are accounted for in the simulation through the effects of ion-neutral collisions and drag forces acting on the dust.

3.3.3 Treatment of Ions

The ions in the simulation are treated as singly ionized neon or argon gas particles. Because the number of ions in a plasma is extremely large, and computation time scales as a factor of N^2, even with the benefit of parallelized computing it is too time-consuming to directly model all the ions. The actual simulated ion are “superions” consisting of around 100-200 individual ions in a cluster. Since the superion has the same charge to mass ratio as an individual ion, it has the same dynamics as a single ion. Ions interact with each other and with the plasma environment. The equation of motion for ions in the DRIAD simulation (Matthews et al. 2020) is given by

$$m_i\ddot{r} = -q_i\vec{E_i} + \vec{F}_{in} \tag{3.1}$$

The two forces, then are the force due to the electric field and the force $\vec{F}_{in}$, which is the force between ions and neutral gas particles. The electric field, which is calculated as $\vec{E} = -\nabla\Phi$, with the potential accounting for the contributions of simulated superions, ions outside the simulation region, dust particles, and any other electric fields present in the simulation, such as the axial electric field that acts along the tube of a DC discharge plasma. When interacting with other ions, the ions are treated as Yukawa particles exhibiting shielding by electrons, so the ion-ion potential is given by

$$\Phi_Y(r_i) = \frac{1}{4\pi\epsilon_0}\sum_j \frac{q_j}{r_{ij}} exp\,(-\frac{r_{ij}}{\lambda_{De}}) \tag{3.2}$$

where q_j is the charge on ion j, r_{ij} is the distance between ion i and ion j, and λ_{De} is the electron Debye length. When ions interact in the electron-devoid region surrounding dust grains, the dust grain potential is given as a bare Coulomb potential:

$$\Phi_C(r_i) = \frac{1}{4\pi\epsilon_0}\sum_d \frac{Q_d}{r_{id}} \tag{3.3}$$

where r_{id} is the separation between each ion and dust particle.

3.3.4 Treatment of Dust

The code treats the dust particles as having the same properties as the melamine-formaldehyde microspheres commonly used in dusty plasma experiments, with a user-specified radius. The dust equation of motion (Matthews et al. 2020) is given by

$$m_d\ddot{x} = \vec{F}_{dd} + \vec{F}_{id} + m_d\vec{g} + Q_d\vec{E} - \beta\dot{x} + \xi r(t) \tag{3.4}$$

for a dust particle with mass m_d and charge Q_d has a force from other dust grains ($\vec{F}_{dd}$), ions ($\vec{F}_{id}$), gravitational force, electric field force, neutral gas drag (βx) and a thermal bath ($\xi r(t)$ that generates random kicks. Each of these forces are found individually as follows. The dust-dust interactions and the force of the dust on ions are approximated to occur in a bare Coulomb potential because of the absence of electrons in the area close to dust grains.

$$\vec{F}_{dd} = \frac{1}{4\pi\epsilon_0}\frac{Q_d q_d}{r^2} \tag{3.5}$$

$$\vec{F}_{id} = \frac{1}{4\pi\epsilon_0} q_i \sum_j \frac{q_j}{r_{ij}^2} \tag{3.6}$$

The force $Q_d\vec{E}$ gives the dust reaction to confinement by electric fields present in the simulation and is given by $Q_d\left(\overrightarrow{E_r} + \overrightarrow{E_z}\right)$. The axial and radial components of the confining force represent the electric field generated by dust particles outside of the simulation region, which keep the dust particles within a specific region. The dust confinement represents the fact that only a small portion of the central region of the dust cloud is simulated.

The neutral gas drag $\beta\dot{x}$ is a drag force proportional to the dust velocity with respect to the neutral gas background, which is present because in the experimental system, not all gas molecules are ionized. The proportionality constant β depends on the pressure and temperature of the neutral gas:

$$\beta = \frac{\delta 4\pi a^2 n m_g}{3m_d}\sqrt{\frac{8k_B T_g}{\pi m_g}} \tag{3.7}$$

where δ = 1.44, experimentally derived for melamine-formaldehyde in argon gas, a is the dust radius, n is the number density of neutral gas, m_g is the molecular mass of the gas, m_d is the dust mass, and T_g is the gas temperature.

The final term in the dust equation of motion, $\xi r(t)$, is the thermal bath that introduces Brownian kicks, simulating the non-equilibrium thermal background. The strength of the kick is characterized by

$$\xi = \sqrt{\frac{2\beta k_B T_g}{m_d \Delta t_d}} \tag{3.8}$$

where Δt_d is the dust timestep and $r(t)$ is a random number drawn from a Gaussian distribution.

1.1.1. Simulated Dust Charging

The dust charge Q_d appears in the dust equation of motion in terms of the ion-dust force, the dust-dust force, and the electric field confinement force. The dust grain charge is calculated for each dust grain by a combined OML and MD approach. The OML theory of dust grain charging, discussed in detail in Chapter 2, determines the electron current to the dust grain, given as

$$I_e = \pi a^2 n_e e \sqrt{\frac{(8k_B T_i)}{\pi m_i}} exp(-\frac{e\Phi}{k_B T_i}) \tag{3.9}$$

where Φ is the dust grain surface potential.

The current of ions to the dust grain is determined by the molecular dynamics part of the simulation, where simulated superions that collide with a dust grain are assumed to stick. These superions are flagged and counted across ion timesteps, with their sum divided by the elapsed time during the ion timesteps constituting the ion current to the dust grain surface. Because the current is evaluated over a shorter interval than the dust timestep, and because each collision with a super-ion represents the collection of hundreds of ions, the fluctuation in the ion current to the dust grain is higher than is physical. Thus the accumulated charge is smoothed over several dust steps. The total charge accumulation during an ion timestep is thus given by $\Delta Q = \Delta Q_{de} + \Delta Q_{di}$, where $\Delta Q_{de} = I_e \Delta t_i$ and $\Delta Q_{di} = I_i \Delta t_i$, for the ion timestep Δt_i. As ions collide with the dust grain surface and are removed from the simulation, the same number of ions are reinserted near the simulation boundary, reflecting the continual ionization of neutral gas in the powered plasma system. Ions that exit the simulation region are reinserted by the same method.

3.4 Fitting the Model to the Experiment

3.4.1 Representing the PK-4 Through DRIAD

In order to represent the relevant physics in the numerical model, the model uses certain inputs to the code that borrow directly from experimental conditions. As previously discussed, the background plasma conditions are extremely important for determining the behavior of the dust and its ability to self-organize into a structured system. Fast moving ionization waves have long been known to exist in plasmas (Pekarek 1968) but have recently been shown to have an effect on the formation of strings in complex plasmas (Hartmann et al. 2020; L. S. Matthews et al. 2021a; Vermillion et al. 2022). In order to reproduce the background conditions in which ionization waves are present, PIC codes have been used to determine the microsecond-scale variations in electric field and plasma species number density (Hartmann et al. 2020). These parameters have been recorded and read into the simulation, providing the time evolving plasma conditions that are used in the simulation and are discussed in more detail in the following chapter.

In a typical complex plasma experiment, the number of dust grains is on the order of several thousands, and is higher than the number of dust particles included in the DRIAD simulation, but the confinement of the dust particles in the simulation represents the confinement of the dust outside the simulation region. Thus, the simulation effectively models a narrow cylinder along the central axis of the PK4. In other experiments dealing with the investigation of isotropic to string transitions in plasma (Pustylnik et al. 2020), a reduced number of dust particles from this region are chosen for structural analysis. Even though the simulation data includes fewer dust particles, it effectively considers the effects of a more expansive system.

DRIAD carries the option to calculate accelerations due to gravity, but because the PK-4 is a microgravity laboratory, the gravitational forces are negligible and are not calculated. The PK-4 generates a DC powered discharge with polarity switching at 500 Hz, in order trap dust particles in the field of view of cameras used to take data; this polarity switching is also accounted for in the simulation.

CHAPTER 4

4 Numerical Results

4.1 Dust Clouds

4.1.1 Motivation

In microgravity, forces between dust particles are analogous to the interatomic or intermolecular forces in normal matter; characterizing the nature of these dust-dust interactions defines distinct phases. When dust is initially dropped into the plasma system or randomly injected into the simulation, it behaves in a highly disordered “gaseous” state. Dust particles show no real organization or structure in any direction. When particles begin to interact in the simulated system, many complex interactions begin to guide the dust cloud into an equilibrium position. Dust particles collide with ions and electrons in the methods described in the previous chapter, and these collisions bring the dust to an equilibrium surface charge that remains stable for the duration of the simulation. Neutral gas atoms contribute a drag force, damping the motion of dust grains as well as contributing Brownian kicks, simulating the thermal gradients present in the neutral gas background. Rather than collisions driving the system to an overall thermal equilibrium, the kinetic temperatures between dust, ions, and electrons remain distinct. The negatively charged dust particles then introduce local deviations from quasi-neutrality in the plasma background. As ion wakes form around the dust particles, further deviations from neutrality emerge due to the streaming ions, and the changing polarity of the electric field elongates these ion clouds. The shielding effect from ion wakes diminishes the repulsive reaction between dust grains, allowing for unexpected coupling between dust particles as dust particles are attracted to the wakes of neighboring particles.

Electrorheological fluids are a category of materials whose rheology exhibits strong dependence on external conditions. Complex plasmas have been shown to demonstrate electrorheological properties, including the formation of string-like clusters (SLCs) due to applied fields. In electrorheological fluids, the formation of SLCs is thought to be due to long-range attractive forces between charged particles, but the recent publication (Joshi et al. 2023) suggests that rather than long-range attraction, the reduction of long range repulsion between dust particles due to the elongated ion wakes that form in the flowing plasma is enough to effect the formation of SLCs.

After dust grains in the simulated PK-4 reach their equilibrium charge, they begin to form strings along the direction of an externally applied electric field, and a structure of nested cylinders begins to emerge in the radial direction. The phase transitions from random, gas-like structure in the cloud to a more ordered, liquid-like structure is studied qualitatively though analysis in one, two, and three dimensions.

4.2 Simulated Data

In order to look at the pressure dependence of the three-dimensional structure of a microgravity dust cloud, simulations were conducted for plasma conditions at gas pressures of 40 Pa and 60 Pa. 1700 dust grains are randomly placed into the system with positions within a region 0.522 mm x 0.522 mm x 1.40 mm in size and allowed to self-consistently organize against a background of evolving plasma conditions, following the methods of the DRIAD simulation discussed in detail in the previous chapter. Dust is shown in its original positions in Figure 13, showing the initial gaseous state.

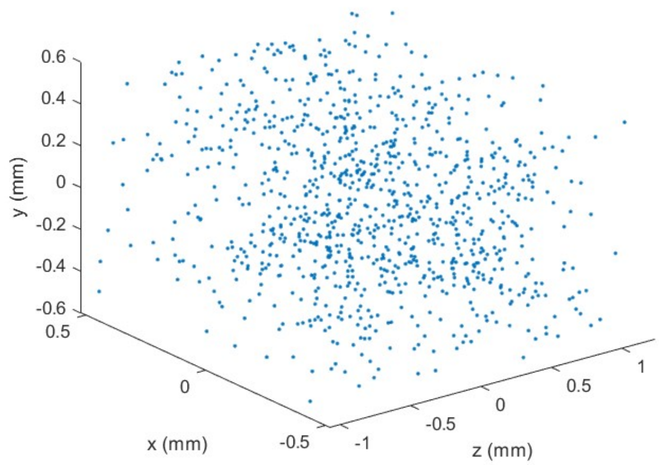

Figure 13: Randomly distributed dust at the beginning of the simulation. During the first few timesteps of the simulation, the dust is highly disordered and resembles a "gaseous" state.

The dust grains are each given an initial charge of $-1.34 \times 10^{-16}\ C$, or $839e$, where e is the charge on an electron. The dust grains rapidly acquire a larger negative charge as they move towards an equilibrium charge and position.

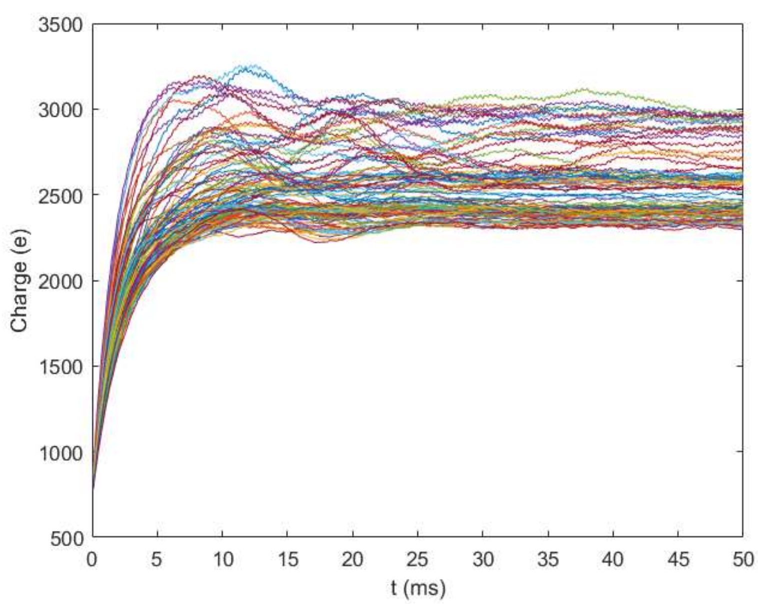

Figure 14: Charge on central dust particles for the first 50 ms. Interaction with the plasma background causes the dramatic increase in dust charge. Several oscillations occur before the equilibrium charge is reached.

After 30-40 ms, the dust particles reach an average equilibrium charge of 2500 e, which remains constant for the duration of the simulation, shown in Figure 14.

Each of the pressures simulated have time-evolving background plasma conditions that are derived from PIC simulation data which reveals the presence of fast-moving ionization waves. These changing parameters account for the presence of microsecond-scale fluctuations in the plasma, which have been shown to significantly enhance the formation of ion wakes and corresponding electrorheological effects (L. S. Matthews et al. 2021b). The background plasma conditions for the 60 Pa case and the 40 Pa case are shown in Figures 14 and 15, respectively.

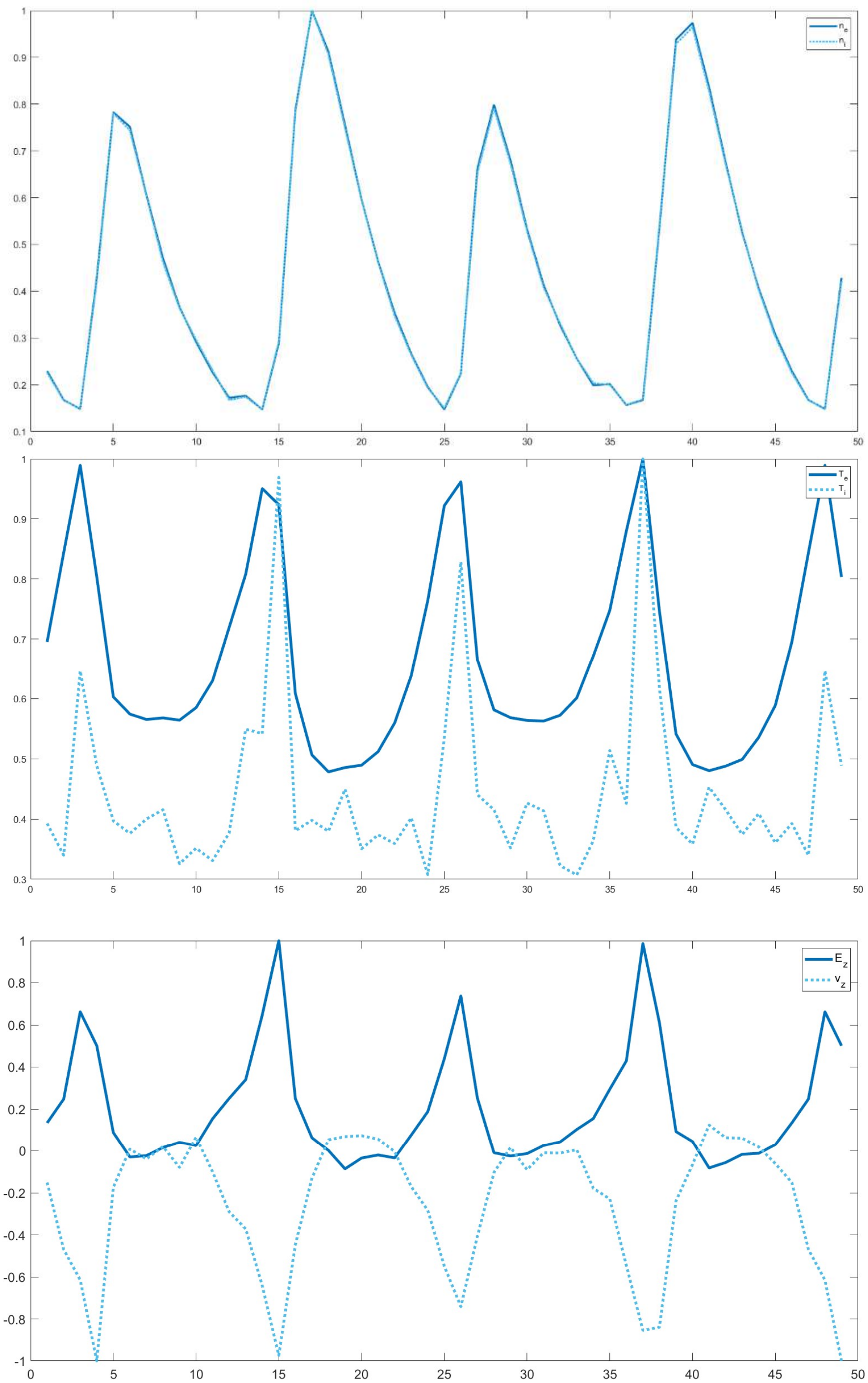

Figure 15: Time evolving plasma parameters for the 60 Pa simulation showing the number density of electrons (n_e) and ions (n_i) (top), electron temperature (T_e), ion temperature (T_i) (middle), and the variation of the electric field strength in the axial (E_z) direction and the drift velocity (bottom).

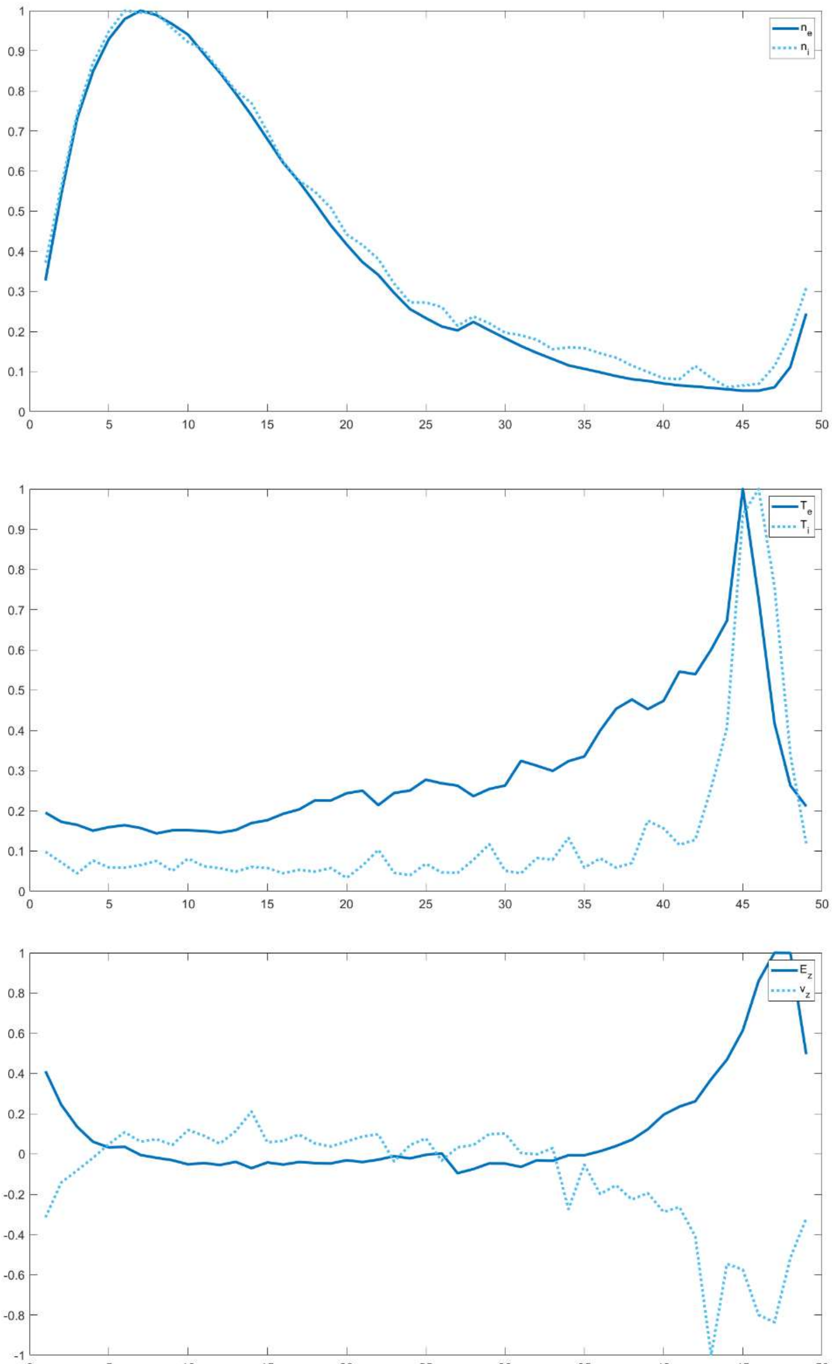

Figure 16: Time evolving plasma parameters for the 40 Pa simulation showing the number density of electrons (n_e) and ions (n_i) (top), electron temperature (T_e), ion temperature (T_i) (middle), and the variation of the electric field strength in the axial (E_z) direction and the drift velocity (bottom).

Dust particles are allowed to evolve in the simulation until they reach an equilibrium position which displays liquidlike order in axial chains, as well as radially spaced nested structures (Figure 16).

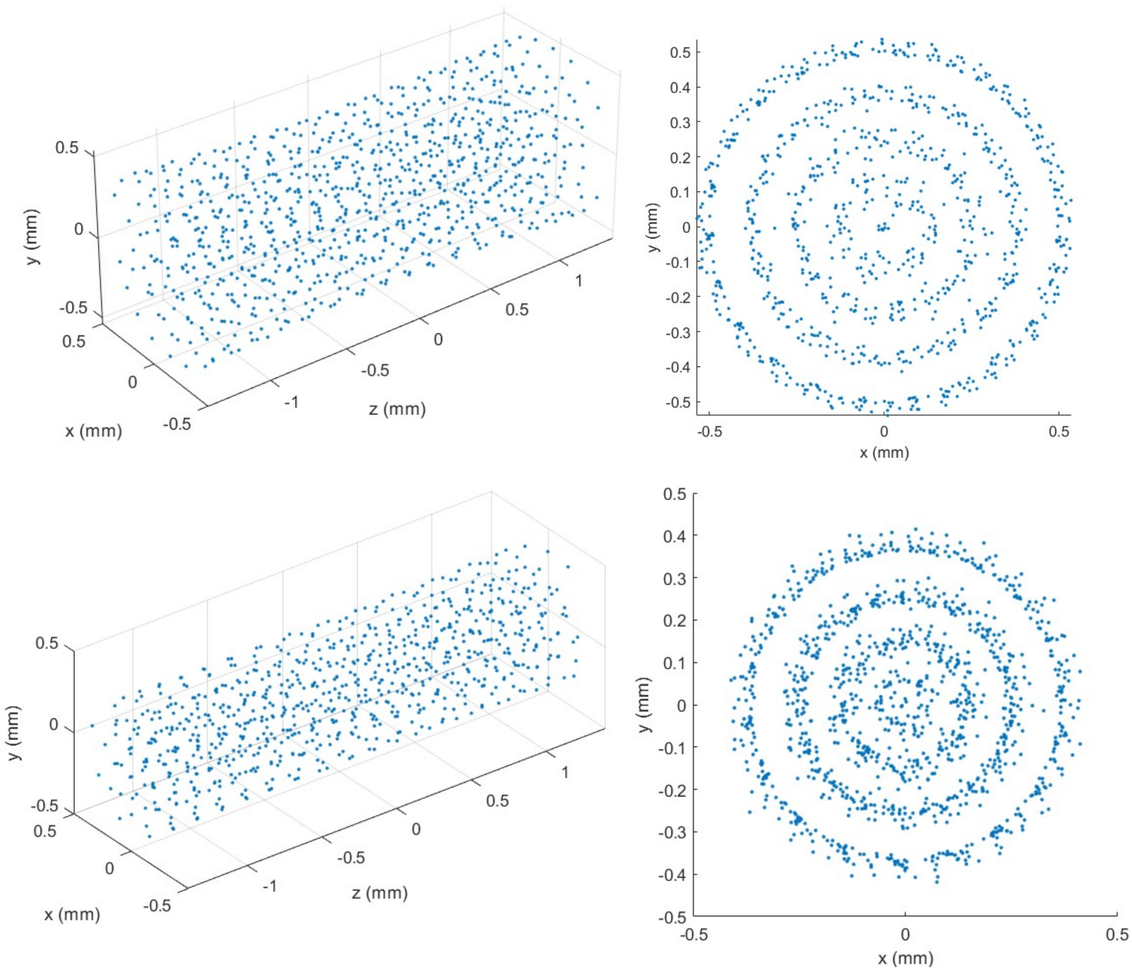

Figure 16: End on view of dust positions at the end of the 60 Pa simulation (top) and the end of the 40 Pa simulation (bottom), after 1.2 seconds.

Axial slices through this cloud reveal the presence of axial dust chains, which are more defined in the central region of the cloud (Figure 17).

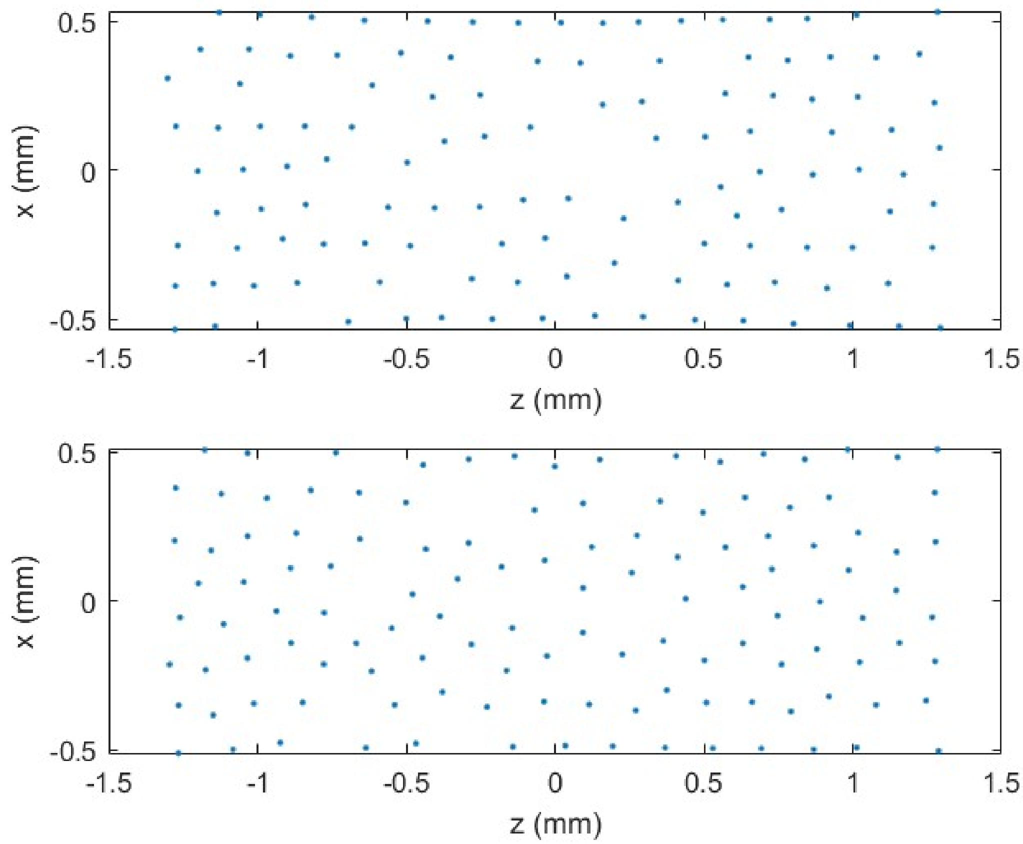

Figure 17: Axial slices 120 μm thick are taken through the 60 Pa dust cloud, after 1.2 s through the center of the cloud (top) and towards the edge of the cloud (bottom).

4.3 Analysis

Over the duration of the simulation, the dust particles move into a stationary configuration that is maintained by the system despite the non-equilibrium conditions. Ions are being continually injected into the simulated system, reflecting the way a laboratory plasma must be maintained with a constant flow of neutral gas that is continually being ionized and recombining with electrons at a steady state. The plasma background is dynamic, but dust particles maintain a stable configuration in the simulation after 1-2 seconds. The difference in dust configuration from the beginning of the simulation to the end indicates a phase transition from a random, gas-like state into a stable state that can by quantitatively studied by examining different parts of the overall dust cloud structure.

4.3.1 The Radial Distribution Function

The pair correlation function, $g(r)$, is a parameter to quantify correlation of particle positions along one or more dimensions. In one dimension, the pair correlation function represents the probability of finding a particle at a certain distance away from a reference point, averaged over all reference particles considered. Higher values of $g(r)$ represent a higher probability of finding a particle a distance r from a given particle. For a perfect crystal where particles are at fixed distance from each other, the pair correlation function will exhibit delta-function peaks, with $g(r) = 0$ apart from the peaks.

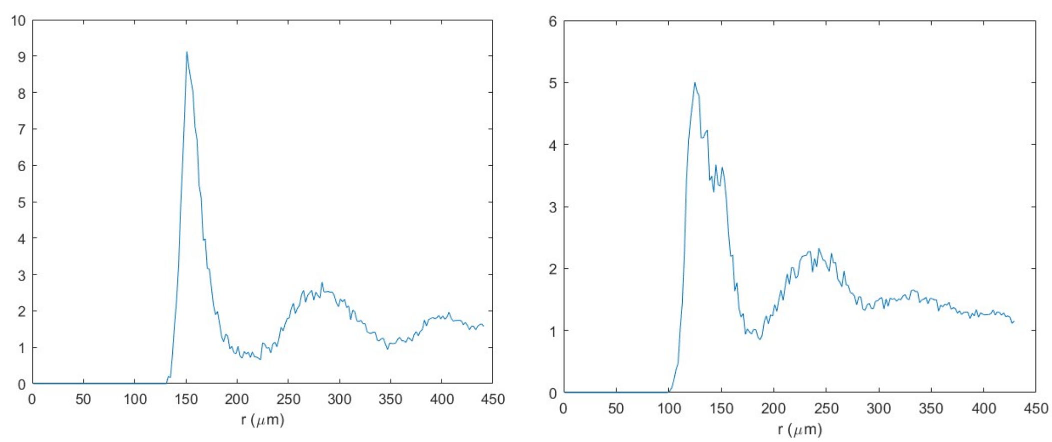

Figure 18: 1-dimensional pair correlation $g(r)$ over entire dust cloud at 60 Pa (left) and 40 Pa (right) that demonstrates liquidlike order. The peaks at 150 and 280 μm indicate the presence of first and second nearest neighbors for each particle considered throughout the cloud at 60 Pa.

In a gaseous system, the pair correlation tends to unity at any separation; there is no preferred spacing between particles. In a liquid-like system, the pair correlation displays peaks at the average interparticle spacing, smoothly transitioning from first to second nearest neighbor until trending to one at large separation. Figure 16 shows the liquid-like correlation of the simulated cloud at 60 Pa and 40 Pa. In the 60 Pa data, the third-neighbor peak is more clearly defined, indicating a higher degree of order in the dust cloud. The liquid-like pair correlation in the dust cloud reflects the presence of axial chains in the dust cloud (Figure 19).

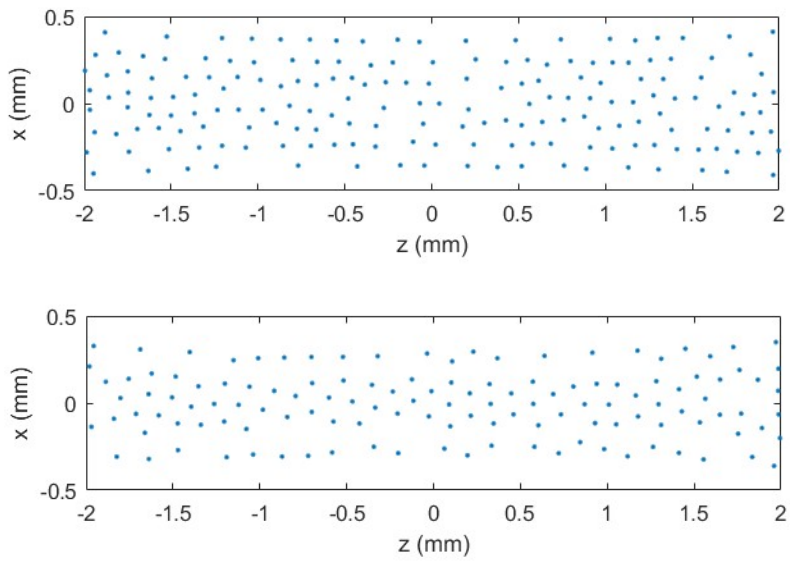

Figure 19: 90 μm thick axial slices showing sections of the xz plane in the 40 Pa cloud near to the center of the cloud (top) and toward the edge of the cloud (bottom).

4.3.2 Three-Dimensional Pair Correlation Functions

In addition to displaying correlation in the radial dimension, indicating preferred values of interparticle spacing, the dust cloud structure on the PK-4 has been shown to display orientational correlation, where dust particle pairs display preferred angular orientations. The three-dimensional structure of the cloud can then be analyzed with pair correlation functions that consider the probability of finding a particle at a particular angular orientation and distance (Pustylnik et al. 2020; Mitic et al. 2021). We define higher order pair correlation functions that compare orientation in a spherical coordinate system in a similar method to (Pustylnik et al. 2020) who defines the 3-dimensional pair correlation:

$$g(r,\theta,\phi) = \frac{1}{n_d N_{ref}} \sum_{\substack{i,j=1 \\ i\neq j}}^{N_{ref}} \frac{\delta(r_{ij}-r)\delta(\theta_{ij}-\theta)\delta(\phi_{ij}-\phi)}{4\pi r^2 \cos(\theta)} \tag{4.1}$$

where the coordinates r_{ij}, θ_{ij}, and ϕ_{ij} describe the vector connecting particle i and particle j from a coordinate system with the origin fixed at particle i, as shown in figure (xx). The coordinates r, θ, and ϕ are spherical coordinates centered on reference particle i. The factor n_d is the number densiry of the dust particles averaged throughout the cloud volume in units of m^{-3}. N_{ref} is the total number of reference particles considered. This differs from the total number of particles in the system because only particles from the central region of the simulated cloud are chosen as reference points to minimized edge effects when normalizing the distribution. When this equation is implemented in MATLAB, the Dirac delta functions are interpreted by binning the data in two dimensions at a time and counting the number of particles which fall inside a bin centered at a given position defined by (r,θ) or (r,ϕ).

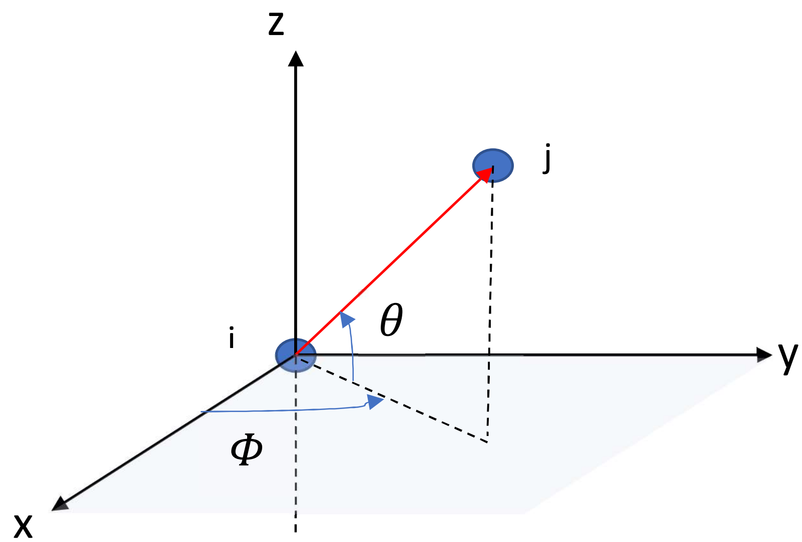

Figure 20: Coordinate system showing the vector r_{ij} in red.

The analysis is conducted in MATLAB by first calculating the vector between each dust particle pair, defined by $\vec{r}_{ij} = \vec{r}_i - \vec{r}_j$, where $\vec{r}_i$ and $\vec{r}_j$ are the positions of the ith and jth particles with respect to some origin (Figure 20).

For each particle i , the polar angle, θ, for $\vec{r}_{ij}$ is defined as the angle measured from the positive z axis, which is parallel to the cylindrical axis of the dust cloud and the direction of the applied electric field. The azimuthal angle, ϕ, of this vector is the angle of the projection in the xy plane, the planes that reveal the cross-sectional nested structure of the cloud. The coordinates are calculated from the positions as:

$$\theta = \sin^{-1}\left(\frac{z}{r}\right) \tag{4.2}$$

$$\phi = \tan^{-1}\left(\frac{y}{x}\right) \tag{4.3}$$

Once the particle pairs are defined, they are sorted using a two-dimensional histogram function in MATLAB, histcounts2, which divides the particle pairs into two-dimensional bins. The data must be normalized carefully with respect to the expected dust density within the volume considered for the pair correlation function. In a typical $g(r)$ pair correlation for 3D data, this normalization volume is taken as the volume of spherical shell corresponding to the r coordinate. When two orientational dimensions are considered, the normalization volume is found by integrating a spherical cuboid over the considered bin dimensions. For the $g_\phi(r,\theta)$ projection, data is binned in r and θ and integrated over all ϕ from 0 to 2π. The associated volume for each bin can be visualized as dividing the total spherical volume into sections of equally spaced θ and equally spaced r; bin volumes look like onion rings. This volume is found by integrating over bin edges:

$$\int_{r_1}^{r_2} r^2\, dr \int_{\theta_1}^{\theta_2} \cos(\theta)\, d\theta \int_0^{2\pi} d\phi \tag{4.4}$$

$$= \frac{r_2^3 - r_1^3}{3}(\sin\theta_2 - sin\theta_1)(2\pi) \tag{4.5}$$

To express this volume in terms of bin widths Δr and $\Delta\theta$, let

$$r_1 \equiv r - \Delta r \tag{4.6}$$

$$r_2 \equiv r + \Delta r \tag{4.7}$$

and

$$\theta_1 \equiv \theta - \Delta\theta \tag{4.8}$$

$$\theta_2 \equiv \theta + \Delta\theta \tag{4.9}$$

where the coordinates r and θ are the coordinates of the center of each bin. Making these substitutions in r gives

$$r_2^3 - r_1^3 = \frac{\Delta r^3}{4} + 3r^3\Delta r \;\approx\; 3r^3\Delta r \tag{4.10}$$

and because the bin widths are sufficiently small, only linear terms in Δr are kept.

Making the substitutions in the θ term,

$$(\sin\theta_2 - sin\theta_1) = \sin\left(\theta + \frac{\Delta\theta}{2}\right) - \sin\left(\theta - \frac{\Delta\theta}{2}\right) \tag{4.11}$$

it is helpful to use the trigonometric identity

$$\sin(A + B) - \sin(A - B) = 2\cos(A)\sin(B) \tag{4.12}$$

so that

$$\sin\left(\theta + \frac{\Delta\theta}{2}\right) - \sin\left(\theta - \frac{\Delta\theta}{2}\right) = 2\cos(\theta)\sin\left(\frac{\Delta\theta}{2}\right) \;\approx \cos(\theta)\,\Delta\theta \tag{4.13}$$

Because bins in θ are sufficiently small, the small angle approximation $\sin(\theta) \approx \theta$ can be used. The total bin volume can now be expressed as:

$$\frac{3r^3\Delta r}{3}\cos(\theta)\,\Delta\theta(2\pi) = 2\pi r^3\cos(\theta)\,\Delta\mathrm{r}\Delta\theta \tag{4.14}$$

For the bin volume associated with the $g_\theta(r,\phi)$ projection, data is binned in r and ϕ and integrated across all θ from $-\frac{\pi}{2}$ to $\frac{\pi}{2}$. For each bin, the r and ϕ coordinates are specified and the θ variable is free to take any value, so the bin volume can be visualized as an

$$\int_{r_1}^{r_2} r^2 dr \int_{-\frac{\pi}{2}}^{\frac{\pi}{2}} \cos(\theta)\,d\theta \int_{\phi_1}^{\phi_2} d\phi \tag{4.15}$$

orange slice. Calculating the volume follows the same steps as above:

$$\int_{r_1}^{r_2} r^2 dr \int_{-\frac{\pi}{2}}^{\frac{\pi}{2}} \cos(\theta)\,d\theta \int_{\phi_1}^{\phi_2} d\phi$$

$$= \frac{r_2^3 - r_1^3}{3}\left(\sin\left(\frac{\pi}{2}\right) - \sin\left(-\frac{\pi}{2}\right)\right)(\phi_2 - \phi_2) \tag{4.16}$$

$$= \frac{r_2^3 - r_1^3}{3}\left(\sin\left(\frac{\pi}{2}\right) - \sin\left(-\frac{\pi}{2}\right)\right)(\phi_2 - \phi_2)$$

Letting

$$\phi_1 \equiv \phi - \Delta\phi \tag{4.17}$$

$$\phi_2 \equiv \phi + \Delta\phi \tag{4.18}$$

and continuing to make the same approximations as above, the volume for the $g_\theta(r, \phi)$ projection can be expressed as

$$2r^2 \Delta r \Delta\phi \tag{4.19}$$

The total normalization factor for each bin is the volume of the bin multiplied by the average particle number density across the dust cloud; this gives the expected number of dust particles in the bin for evenly distributed data. This total pair correlation function is then found by averaging over the number of reference particles considered.

In figures 19 and 20, the two different projections of the 3D pair correlation function are shown for each pressure. Each projection demonstrates clear order for the first nearest neighbor indicated by the bright vertical stripe at $r = 180\ \mu m$ in the 60 Pa case and at $r = 140\ \mu m$ in the 40 Pa case.

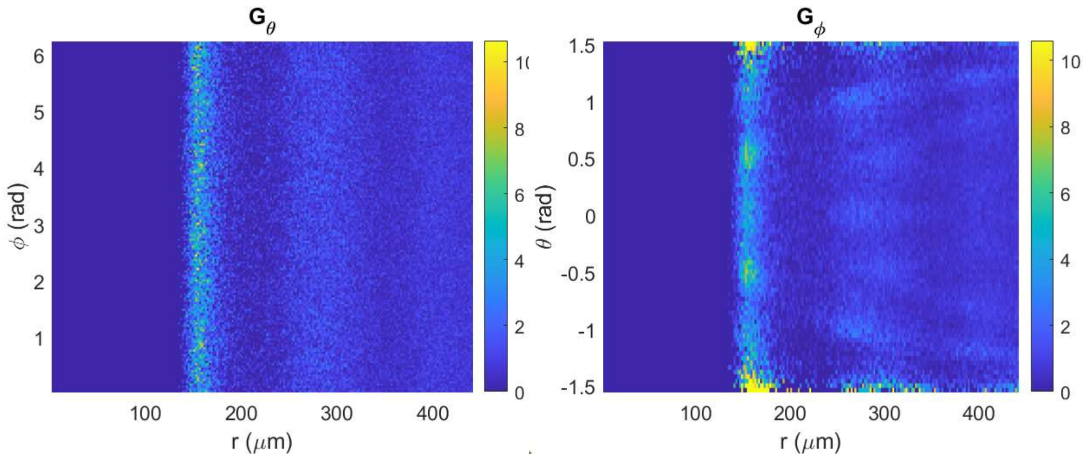

Figure 21: $G_\theta(r, \phi)$ projection of the three-dimensional pair correlation function (left) and $G_\phi(r, \theta)$ projection (right) for simulated data at 60 Pa.

Order decreases as the radial distance increases throughout the cloud, indicated by the decreasing brightness of the second and third subsequent stripes, which correspond to the second- and third-nearest neighbor. In the G_θ projection, the radial peaks are blurred across the ϕ distribution, indicating azimuthal symmetry with no preferred ϕ orientation over the cloud taken as a whole.

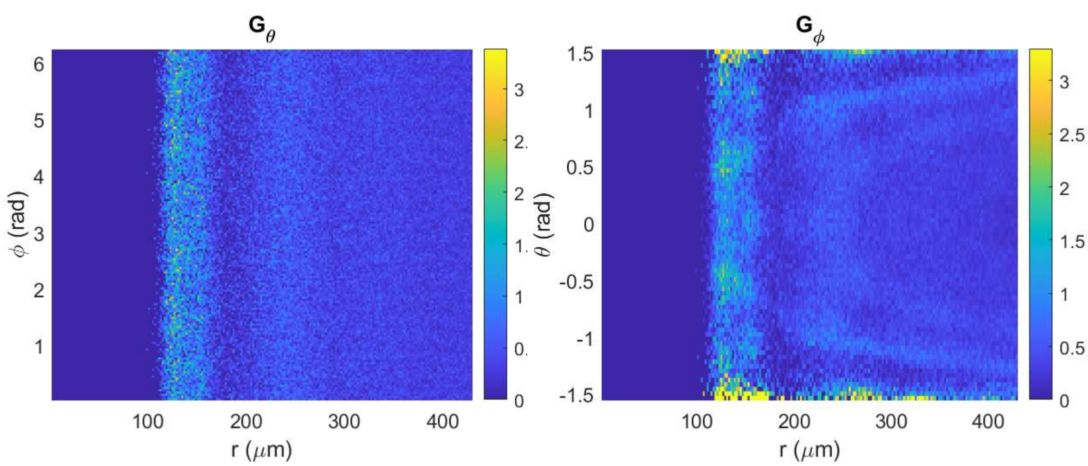

Figure 22: $G_\theta(r, \phi)$ projection of the three-dimensional pair correlation function (left) and $G_\phi(r, \theta)$ projection (right) for simulated data at 40 Pa.

The bright peaks in the G_ϕ projection indicate the chain like order in the axial direction; the bright peaks indicate that it is far more likely to find particle pairs oriented along the axial direction, at $\theta = \pm\frac{\pi}{2}$, than at other orientations. Fainter peaks at $\theta = \pm\frac{\pi}{6}$ indicate that nearest-neighbors often align themselves at $\theta = \pm\frac{\pi}{6}$, if they are not aligned in the axial direction. As radial spacing increases, fainter peaks show up at offset angles, creating a series of arches in the G_ϕ projection which are evidence of the nested structure of the cloud. A preferred orientation in θ arises because of the separation of the cloud into rings.

4.3.3 *Examining Nested Structure*

In addition to analyzing the overall cloud structure, it is useful to isolate and examine parts of the cloud where local order is observed, such as in the nested rings or in the axial chains. Figure 21 shows the end-on views of each simulated cloud, where the individual rings are highlighted.

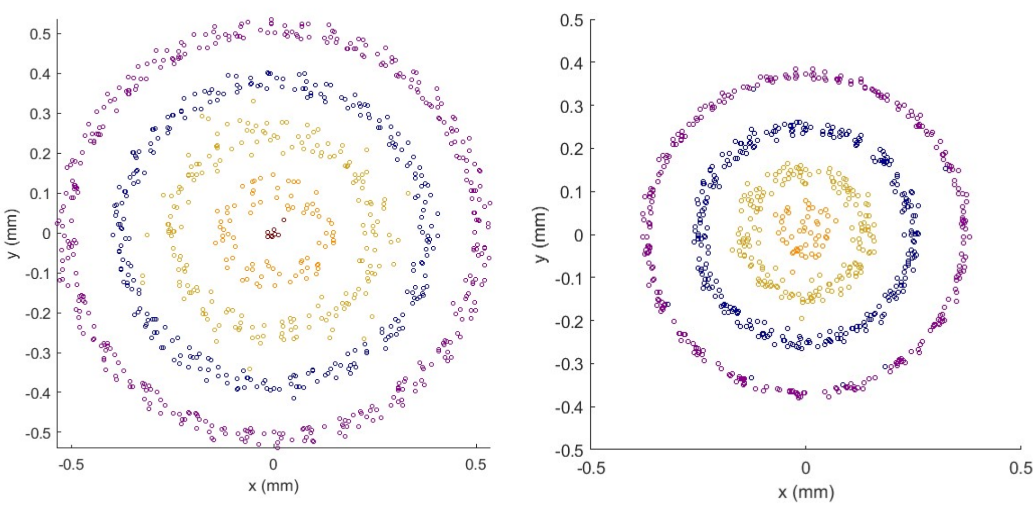

Figure 23: End on view of the dust cloud at 60 Pa (left) reveals 5 nested layers. The dust cloud at 40 Pa is more compact and reveals 4 nested layers.

Isolating individual rings reveals that at both pressures, the dust particles demonstrate crystalline order within the rings, with the outer rings exhibiting clearer crystal structure.

In order to visualize the crystal structures apparent in the individual rings, the distance from the central axis and position along the ring circumference is calculated for each particle. Plotting r against the circumference position, $s = r\phi$, depicts the "unwrapped" cylindrical structure, where the crystal structure of the outer layer is readily apparent. Each particle is sorted into a ring and indexed by its ring position, where the colors correspond to the individual unwrapped cylinders as highlighted in Figure 21.

The classification of order is determined by Delauny triangulation and the complex bond order parameter

$$G_6(j) = \frac{1}{6}\sum_{l=1}^{N_j} \exp(\, i6\Theta_j(l)) \tag{4.20}$$

where N_j is the number of true nearest neighbors of particle j, determined by the Delauny triangulation function. The angle $\Theta_j(l)$ is the angle the vector between particle j and its l^{th} nearest neighbor makes with the positive x axis. For perfect hexagonal structure, the magnitude of the bond order correlation tends to unity. The bond order correlation is calculated for each unwrapped layer of the simulated cylinders, indicating clear hexagonal structure in the outermost layer (Hartmann et al. 2010; E. G. Kostadinova et al. 2021). For the simulated cloud at 60 Pa, the dust forms a nearly perfect crystal with only a few boundaries between the ordered crystalline regions (Figure 24).

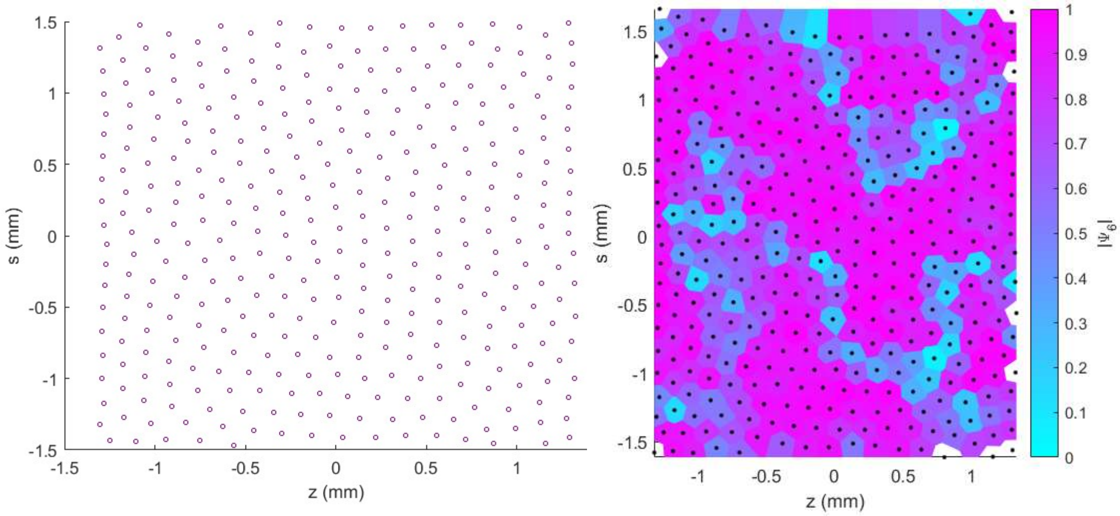

Figure 24: Unwrapped positions of the outermost layer (layer 4) of the simulated cloud at 60 Pa (left). The hexagonal crystal structure is depicted (right) where the color scale indicates the orientation of the nearest-neighbor bonds.

For both pressures, the crystal structure is clear in the outermost shell and decreases as radial distance decreases. Figure 25 shows the first inner layer of the 60 Pa cloud. From the Voronoi diagram, it is easy to see the hexagonal structure is far less prominent in this layer. The patches of clear structure are smaller in this inner layer. Figure 26 and Figure 27 show the next two inner layers, showing increasing deviation from the hexagonal lattice.

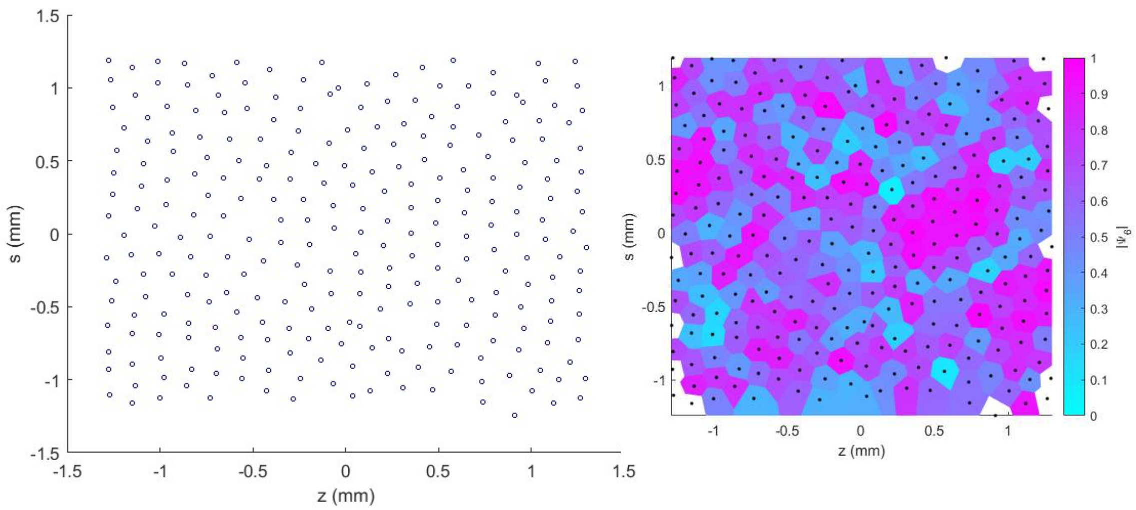

Figure 25: Unwrapped positions of layer 3 in the simulated cloud at 60 Pa (left). The hexagonal crystal structure is depicted (right) where the color scale indicated deviation from perfect hexagonal structure.

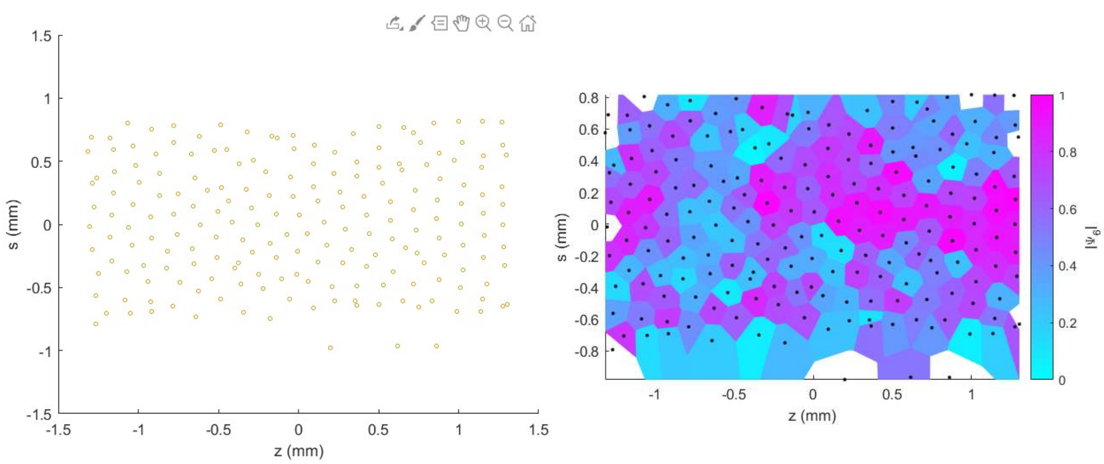

Figure 26: Unwrapped positions of layer 2 in the simulated cloud at 60 Pa (left). The hexagonal crystal structure is depicted (right) where the color scale indicated deviation from perfect hexagonal structure.

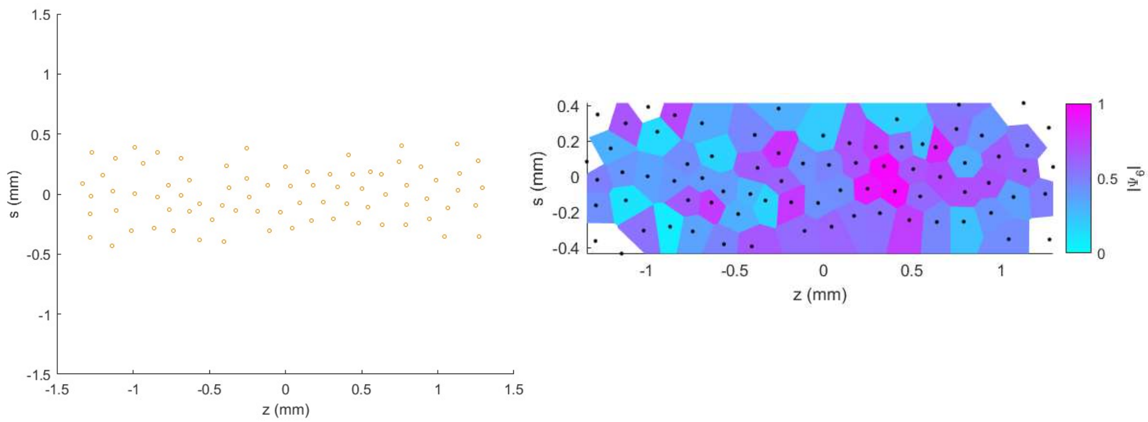

Figure 27: Unwrapped positions of innermost layer (layer 1) in the simulated cloud at 60 Pa (left). The hexagonal crystal structure is depicted (right) where the color scale indicated deviation from perfect hexagonal structure.

The simulated cloud at 40 Pa displays the same trend as the 60 Pa cloud for the crystalline structure of the nester layers, with order increasing with each radial shell. Unwrapped layers are shown in Figure 28 and the corresponding Voronoi diagrams are shown in Figure 29 for the outer three layers.

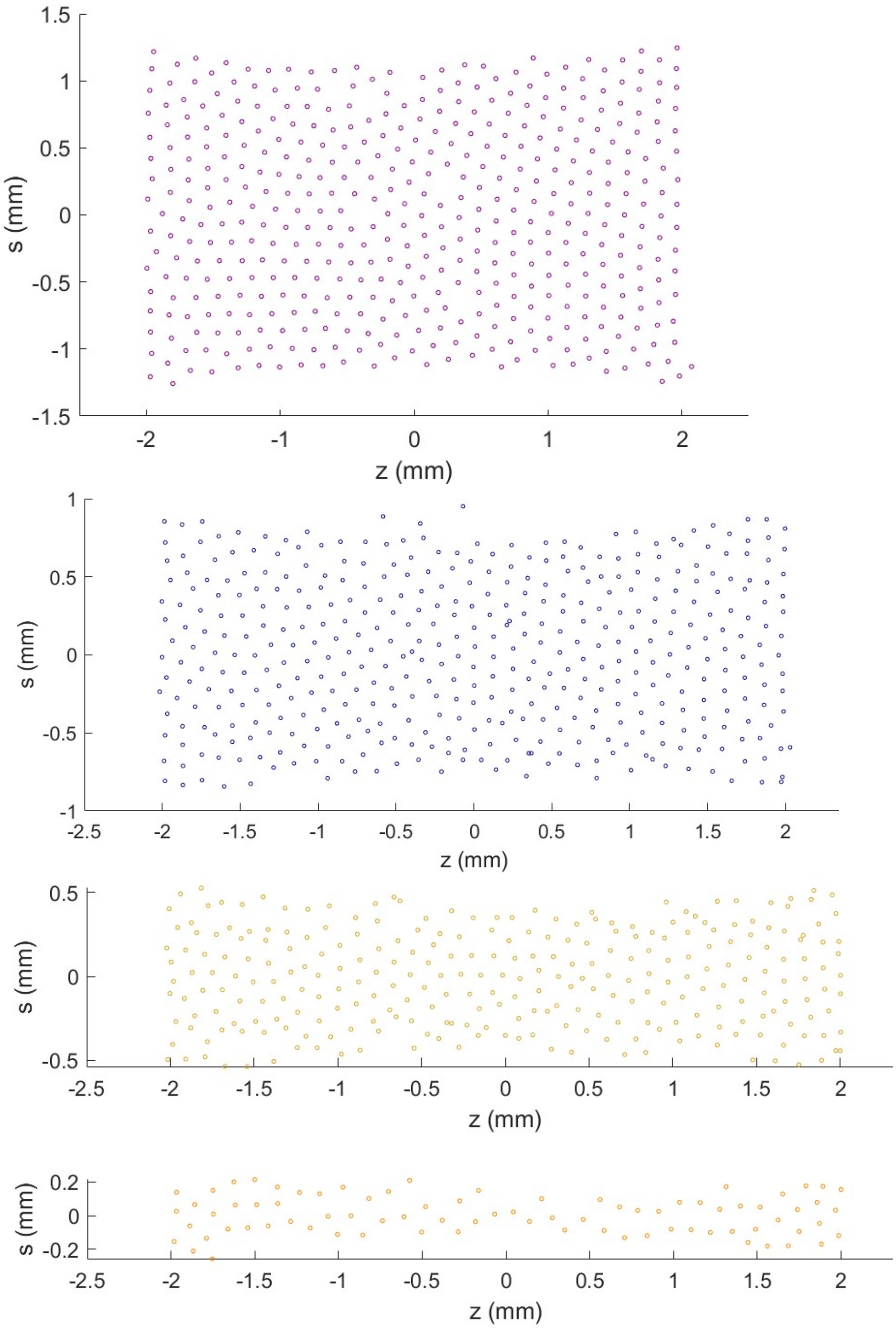

Figure 28: Unwrapped cylindrical layers in the 40 Pa simulated dust cloud.

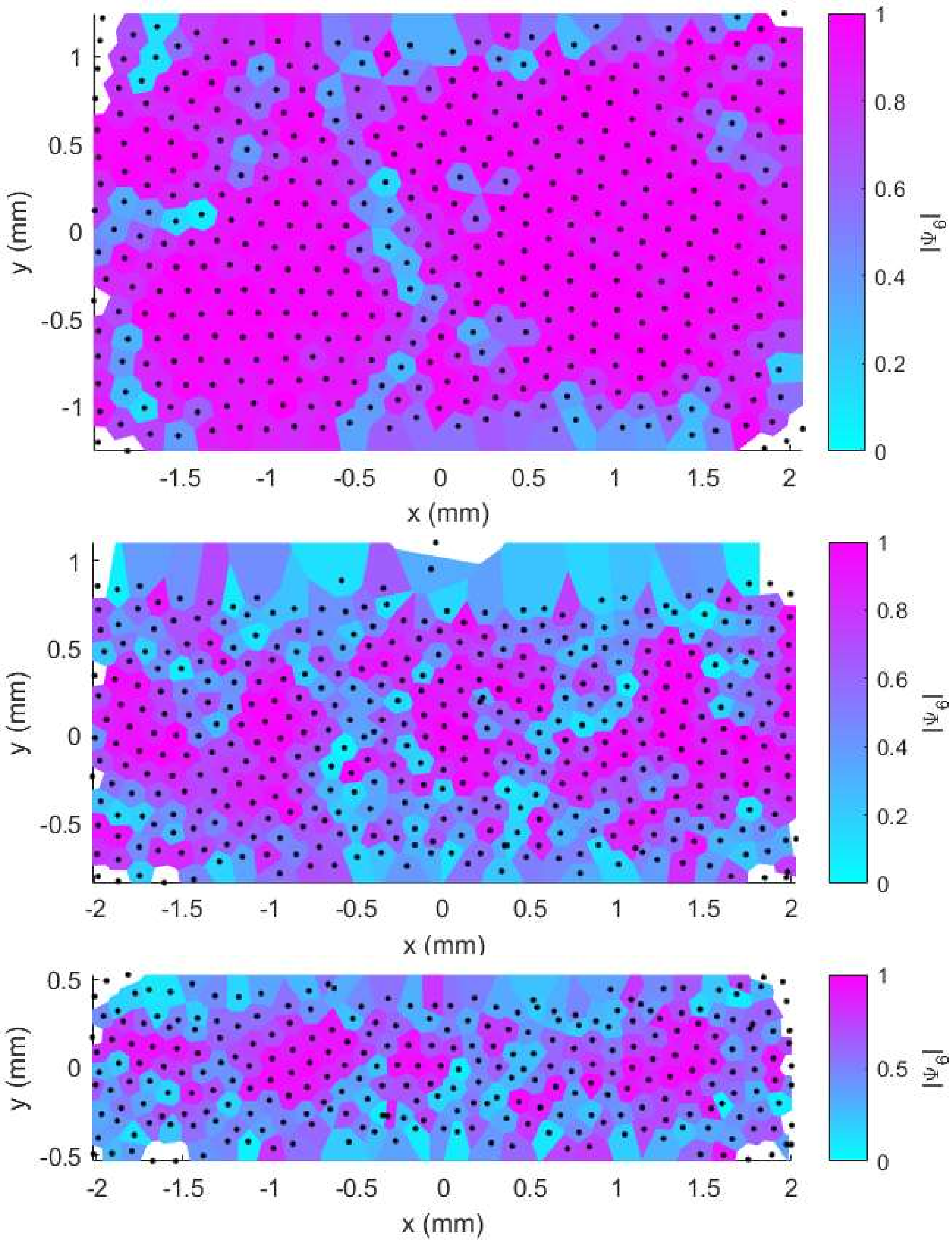

Figure 29: Voronoi diagrams showing the hexagonal lattice structure for the three outermost layers of the unwrapped dust cloud at 40 Pa.

4.4 Conclusions

The DRIAD simulation was used to simulate two different dust clouds, one at a pressure of 40 Pa and one at 60 Pa. Each cloud reveals similar overall cloud structure, with axial chains, SLCs, and a nested structure. Overall liquidlike order is observed through the pair correlation function $g(r)$ for each pressure, with the high-pressure case displaying slightly more defined peaks, indicating higher pair correlation.

Analyzing the pair correlation in terms of angular orientation though the functions $g_{\phi}(r,\theta)$ and $g_{\theta}(r,\phi)$ usefully identifies and quantifies the degree of order in the nested structure of the cloud. The cloud formed at a pressure of 60 Pa shows more defined nested structure, seen though preferred orientations in the θ direction. It was expected to find clear peaks every 60º in the ϕ direction, indicating hexagonal lattice structure in the faces perpendicular to the cylindrical axis. No preferred orientation was found in the ϕ direction, indicating that although the axial chains are present, they are twisted or curve around the z-axis, masking any clear symmetry. This could be an artifact of the duration of the simulation, and it is possible that a longer simulation would allow time for the dust chains to form this hexagonal structure in the xy plane.

Though SLCs are observed as axial chains and are readily observed in slices in the xz plane, the chains are not very long, and there are gaps. A higher degree of string-like order may also emerge with a longer simulation. The nested structure of the dust cloud is well defined at both pressures, and both cases demonstrate very clear hexagonal crystal structure in the outermost unwrapped layer of the dust cloud.

CHAPTER 5

5 A Concluding Reflection on Analogies in Science

Complex plasmas are very interesting systems, but it is worth inquiring about what else makes these systems worth studying, since they are not obviously connected to useful applications like medical or technological advancements. Why should anyone care about self-organizing dust particles in plasmas? For the non-physicist, the minutiae of the mechanics of such an oddly specific system may seem totally detached from the important questions of science, and even for the physicist, the motivations for this research may not be fully apparent. To this end, it is illuminating to consider one of the primary methods used for understanding the phase transitions in the dust cloud. When the dust undergoes a "phase transition" from a disordered, gas-like state to a more ordered liquidlike state, the language we use draws a direct analogy to what occurs in a commonplace phase transition: the condensation of a gas into a liquid. The choice of analogous language is useful for teaching and learning because it situates an unfamiliar phenomenon in terms of a familiar process. Further, it implies that there is something physically similar between the condensation of gases into liquids and the phase transition undergone by the dust cloud.

Analogies are ubiquitous in physics and the language used in physics. Some of these analogies are language-based, with no clear connection to reality. As an example, the "color charge" associated with quarks has absolutely nothing to do with the physical phenomenon of color, but there is still an analogy that aids understanding. Quarks only bind in a color singlet, such the presence of a red, green, and blue quark together, which is analogous to the way red, green, and blue light makes white light. Other analogies in physics are language-based as well as reality-depicting; they imply a physical model. For example, when students learn the harmonic oscillator system for the first time, the model systems of a simple pendulum and of a mass on a spring are often introduced simultaneously. They can be discussed in similar language – the formalism of harmonic oscillators – and they are also mathematically equivalent. So, a distinction can be made between two types of analogy in physics: those that are analogous in language primarily, and those that are also analogous mathematically. I argue that the phase transition undergone by the complex plasma system is analogous in name and also in nature, and that the mathematics and underlying theory of these transitions can be useful in describing the transitions in analogous systems that include self-organization in a wide range of complex systems on many scales.

To lay a more detailed framework for the importance of analogies in physics, it is helpful to focus on two primary uses of metaphors in physics: pedagogical-conceptual and mathematical. First, analogies carry great pedagogical power, because they place the unfamiliar and new in terms of something already known by a student. With respect to teaching and learning, the philosopher John Dewey articulates a tension between the mode of education as "development from within" as opposed to "formation from without," but articulates the progressive view of education as one that emphasizes the intimate connection between knowledge and experience (Dewey 1938). According to Dewey, understanding is derived from experience, and so a child's education is hindered by the traditional mode of passing down mere content, rather than allowing the child to take part in the learning itself. The theory of experiential learning works well for certain types of learning and is often implemented in science education even at the college level – I think of the introductory physics labs offered at Baylor – but much of modern science is necessarily beyond experience.

The limitations of experience of concepts in physics necessitates teaching by way of analogy. Certain physical processes take place in the experiential, familiar realm – for example, the concept of gravitational force. Though "force" and "gravity" may be unfamiliar terms, the phenomenon itself is very familiar – it makes things fall down. However, other physical processes are not experiential – for example, the process of turning on a light. Though everyone has flipped a light switch, there is nothing about the experience of flipping the switch that indicates what is happening with the underlying physics. Even the most inquisitive light switch operator, who may have removed the cover of the switch to observe the wiring, and who may understand that a complete circuit is required for the light to turn on, will not be able to tell by his or her experience what causes electricity to flow. However, for the first encounter with the concept of electric current in circuits, analogies to water flowing in a pipe are often used to help the learner map a non-experiential phenomenon onto something familiar. Just as water flows downhill, electric current "flows" down a potential gradient. Kirchoff's laws for currents can be introduced through the water analogy very well, on a conceptual level. So, "experiential learning" can be usefully extended through analogical comparisons.

While the first use of analogies in physics is primarily conceptual, and most useful on a general scale, mathematical analogies deepen and enhance the importance of analogies in physics by creating models that are applicable to a wide range of physical systems. As Mary Hesse discusses in her work *Models and Analogies in Science*, the concept of “waves” in physics begins as a language based analogy, but incidentally carries an identical mathematical formalism between all things called “waves” (Hesse 1966) . The shared language of waves, in addition to the shared mathematical descriptions, is an analogy that exists in the theoretical model of all waves – transverse or longitudinal, light, sound, or water. Important distinctions of course exist between the different types of waves, but the analogy remains descriptively useful.

Before applying each of these concepts directly to the focus of this thesis, the phase transitions observed in complex plasmas, it should be qualified that attempts at analogous understanding can be misleading if they are not carefully limited in scope and application. To use the language of Hesse, for any model there are both “positive analogies” and “negative analogies” which mark the important similarities and differences, respectively, between a known model system and the system on inquiry. To draw an analogy is not to assume that all connections are of the “positive” type; identification of the negative analogical aspects strengthens the predictive nature of the model.

Within Hesse’s philosophical framework, what is the model associated with complex plasmas? First, there are connections between the plasma and a fluid. When Langmuir originally coined the term “plasma,” it was in the predictive-model sense described by Hesse. Though the new system of the “plasma” was unknown, it was similar important ways to blood plasma in that it was fluidlike, it carried and distributed impurities. The name “plasma” was chosen not out of Langmuir’s lack of creativity, but out of a motivation to think and talk about plasmas in a way that was grounded in the familiar understanding of blood in the human body but also welcomed extending of the theory surrounding the new state of matter.

In addition to being fluidlike, plasmas are also said to be conducting fluids; they exhibit similar electrical properties of conducting metals like the ability to shield out deviations from charge neutrality over large enough characteristic distances. So, the model for plasmas is extended: not only a fluid, but also a conducting fluid. Other related mechanical analogies have been shown to exist with respect to complex plasmas, including the connection to electrorheological (ER) fluids. ER fluids are those whose material properties show extreme sensitivity to external conditions like applied fields; ER plasmas exhibit different viscosities and order based on the applied electric fields.

Additionally, there are connections between liquid crystals (LC) and complex plasmas. Rod-like LC particles look like the elongated dust-plus-wake particles present in alternating field plasmas. The liquidlike phases exhibited by dust clouds in the PK-4 are similar to the LC nematic and smectic phases (Evdokiya G. Kostadinova et al. 2023). The analogy between complex plasmas and liquid crystals welcomes a theoretical exploration of LC universality in its relation to complex plasma phases. Mary Hesse's assertion is that models and analogies in science are not only prevalent and more valid than is generally thought, and that extensions of models contribute to a sort of scientific imagination that is positive for developments in theory is exemplified by the numerous analogies associated with complex plasmas.

The framework of thinking about physics analogically and creatively welcomes an interdisciplinary inquiry that has recently become increasingly popular even among hard sciences. The need for scientific disciplines to be in conversation with each other for specific projects – such as initiatives for materials science, artificial intelligence (AI) applications, or biophysics – is counter to the specialist-reductionist approach to scientific innovation. In order to make progress toward understanding increasingly complex systems, the detailed knowledge of the specialist can be productively paired with the scientific imagination about the broad connections between seemingly distinct disciplines to extend theory in relevant ways.

Similar to the way that complex plasmas may understood in connection to other model systems, complex plasmas may also be used as model systems for more complex and hard-to-study systems, such as the self-organizing systems that are vital to the function of the human body. A deeper understanding of the fundamental physics of self-organizing systems through the model system of complex plasmas may be extremely useful for tackling questions in biophysics: how are drugs transported through the body, and how could these trajectories be tuned to increase drug efficacy? How is relevant information transmitted between cells that make decisions regarding immune responses? How are self-organizational functions inhibited or affected by cancer? All of these questions, though of course distinct from the field of plasma physics, are incredibly complex from a reductionist approach; extensions of analogy from the simpler system of complex plasma could provide breakthroughs in medical technology that could save lives.

Future computational investigations of complex plasmas include drawing more explicit connections between plasmas and the analogous LC, soft matter, or living systems. Improved computational methods that utilize artificial intelligence as well as GPU computing could greatly increase the capacity for complexity in plasma models, as well as decrease the cost of simulations that can run over longer timescales. The future of complex plasma research as a model system for some of the most exciting frontiers of science could make it an avenue for scientific imagination and collaboration that I hope will be furthered by my generation of scientists.

BIBLIOGRAPHY

Allen, J. E. 1992. “Probe Theory - the Orbital Motion Approach.” *Physica Scripta* 45 (5): 497. https://doi.org/10.1088/0031-8949/45/5/013.

Bechinger, Clemens, Roberto Di Leonardo, Hartmut Löwen, Charles Reichhardt, Giorgio Volpe, and Giovanni Volpe. 2016. “Active Particles in Complex and Crowded Environments.” *Reviews of Modern Physics* 88 (4): 045006. https://doi.org/10.1103/RevModPhys.88.045006.

Brake, M. L., J. Pender, and J. Fournier. 1999. “The Gaseous Electronic Conference (GEC) Reference Cell as a Benchmark for Understanding Microelectronics Processing Plasmas.” *Physics of Plasmas* 6 (5): 2307–13. https://doi.org/10.1063/1.873482.

Chaubey, Neeraj, and J. Goree. 2022a. “Coulomb Expansion of a Thin Dust Cloud Observed Experimentally under Afterglow Plasma Conditions.” *Physics of Plasmas* 29 (11): 113705-. https://doi.org/10.1063/5.0112680.

———. 2022b. “Coulomb Expansion of a Thin Dust Cloud Observed Experimentally under Afterglow Plasma Conditions.” *Physics of Plasmas* 29 (11): 113705. https://doi.org/10.1063/5.0112680.

Chen, Francis F. 2016. *Introduction to Plasma Physics and Controlled Fusion*. 3rd ed. Switzerland: Springer International Publishing.

Chu, J. H., and Lin I. 1994. “Direct Observation of Coulomb Crystals and Liquids in Strongly Coupled Rf Dusty Plasmas.” *Physical Review Letters* 72 (25): 4009–12. https://doi.org/10.1103/PhysRevLett.72.4009.

Dewey, John. 1938. *Experience and Education*. The Kappa Delta Pi Lecture Series [No. 10]. New York: The Macmillan company.

Dietz, Christopher, Johannes Budak, Tobias Kamprich, Michael Kretschmer, and Markus H. Thoma. 2021. “Phase Transition in Electrorheological Plasmas.” *Contributions to Plasma Physics* 61 (10): e202100079. https://doi.org/10.1002/ctpp.202100079.

Goertz, C. K., and G. Morfill. 1983. “A Model for the Formation of Spokes in Saturn’s Ring.” *Icarus* 53 (2): 219–29. https://doi.org/10.1016/0019-1035(83)90143-4.

Gurnett, Donald A., and Amitava Bhattacharjee. 2017. *Introdustion to Plasma Phyiscs. With Space, Laboratory and Astrophysical Applications*. 2nd ed. Cambridge: Cambridge University Press.

Hartmann, Peter, Angela Douglass, Jorge C. Reyes, Lorin S. Matthews, Truell W. Hyde, Anikó Kovács, and Zoltán Donkó. 2010. "Crystallization Dynamics of a Single Layer Complex Plasma." *Physical Review Letters* 105 (11): 115004. https://doi.org/10.1103/PhysRevLett.105.115004.

Hartmann, Peter, Marlene Rosenberg, Zoltan Juhasz, Lorin S. Matthews, Dustin L. Sanford, Katrina Vermillion, Jorge Carmona Reyes, and Truell W. Hyde. 2020. "Ionization Waves in the PK-4 Direct Current Neon Discharge." *Plasma Sources Science and Technology*, September. https://doi.org/10.1088/1361-6595/abb955.

Hayashi, Yasuaki Hayashi Yasuaki, and Kunihide Tachibana Kunihide Tachibana. 1994. "Observation of Coulomb-Crystal Formation from Carbon Particles Grown in a Methane Plasma." *Japanese Journal of Applied Physics* 33 (6A): L804. https://doi.org/10.1143/JJAP.33.L804.

Hesse, Mary B. 1966. "Models and Analogies in Science." *Philosophy and Rhetoric* 3 (3): 190–91.

Ikezi, Hiroyuki. 1986. "Coulomb Solid of Small Particles in Plasmas." *The Physics of Fluids* 29 (6): 1764–66.

Introduction to Plasma Physics and Controlled Fusion. n.d. Accessed January 5, 2023. https://link.springer.com/book/10.1007/978-3-319-22309-4.

Ivlev, A. V., G. E. Morfill, H. M. Thomas, C. Räth, G. Joyce, P. Huber, R. Kompaneets, et al. 2008. "First Observation of Electrorheological Plasmas." *Physical Review Letters* 100 (9): 095003. https://doi.org/10.1103/PhysRevLett.100.095003.

Ivlev, A. V., J. Bartnick, M. Heinen, C.-R. Du, V. Nosenko, and H. Löwen. 2015. "Statistical Mechanics Where Newton's Third Law Is Broken." *Physical Review X* 5 (1): 011035. https://doi.org/10.1103/PhysRevX.5.011035.

Joshi, E., M. Y. Pustylnik, M. H. Thoma, H. M. Thomas, and M. Schwabe. 2023. "Recrystallization in String-Fluid Complex Plasmas." *Physical Review Research* 5 (1): L012030. https://doi.org/10.1103/PhysRevResearch.5.L012030.

Khrapak, A.G., V.I. Molotkov, A.P. Nefedov, V.M. Torchinsky, and K. Yoshino. 1999. "Liquid and Crystalline Structures in Dusty Plasmas: Dust Liquid Crystal." In *Proceedings of 1999 IEEE 13th International Conference on Dielectric Liquids (ICDL'99) (Cat. No.99CH36213)*, 657–60. https://doi.org/10.1109/ICDL.1999.799021.

Kostadinova, E. G., R. Banka, J. L. Padgett, C. D. Liaw, L. S. Matthews, and T. W. Hyde. 2021. "Fractional Laplacian Spectral Approach to Turbulence in a Dusty

Plasma Monolayer." *Physics of Plasmas* 28 (7): 073705. https://doi.org/10.1063/5.0047649.

Kostadinova, Evdokiya G., Emerson Gehr, Bradley Andrew, Lorin S. Matthews, Truell W. Hyde, and Abbie Terrell. 2023. "Liquid Plasma Crystals on the ISS." In *AIAA SCITECH 2023 Forum*. AIAA SciTech Forum. American Institute of Aeronautics and Astronautics. https://doi.org/10.2514/6.2023-2615.

Langmuir, Irving, C. G. Found, and A. F. Dittmer. 1924. "A New Type of Electric Discharge: The Streamer Discharge." *Science* 60 (1557): 392–94.

Ludwig, Patrick, Wojciech J. Miloch, Hanno Kählert, and Michael Bonitz. 2012. "On the Wake Structure in Streaming Complex Plasmas." *New Journal of Physics* 14 (5): 053016. https://doi.org/10.1088/1367-2630/14/5/053016.

Matthews, L. S., K. Vermillion, P. Hartmann, M. Rosenberg, S. Rostami, E. G. Kostadinova, T. W. Hyde, et al. 2021a. "Effect of Ionization Waves on Dust Chain Formation in a DC Discharge." *Journal of Plasma Physics* 87 (6). https://doi.org/10.1017/S0022377821001215.

———. 2021b. "Effect of Ionization Waves on Dust Chain Formation in a DC Discharge." *Journal of Plasma Physics* 87 (6): 905870618. https://doi.org/10.1017/S0022377821001215.

———, Dustin L. Sanford, Evdokiya G. Kostadinova, Khandaker Sharmin Ashrafi, Evelyn Guay, and Truell W. Hyde. 2020. "Dust Charging in Dynamic Ion Wakes." *Physics of Plasmas* 27 (2): 023703. https://doi.org/10.1063/1.5124246.

Melzer, André. 2019. *Physics of Dusty Plasmas: An Introduction*. 1st ed. 2019 edition. Cham, Switzerland: Springer.

Merlino, Robert L., and John A. Goree. 2004. "Dusty Plasmas in the Laboratory, Industry, and Space." *PHYSICS TODAY.* 57 (7): 32–39.

Mitic, S., M. Y. Pustylnik, D. Erdle, A. M. Lipaev, A. D. Usachev, A. V. Zobnin, M. H. Thoma, et al. 2021. "Long-Term Evolution of the Three-Dimensional Structure of String-Fluid Complex Plasmas in the PK-4 Experiment." *Physical Review E* 103 (6): 063212. https://doi.org/10.1103/PhysRevE.103.063212.

Morfill, G. E., and H. M. Thomas. 2005. "Spoke Formation under Moving Plasma Clouds—The Goertz–Morfill Model Revisited." *Icarus* 179 (2): 539–42. https://doi.org/10.1016/j.icarus.2005.08.008.

———., and Alexei V. Ivlev. 2009. "Complex Plasmas: An Interdisciplinary Research Field." *Reviews of Modern Physics* 81 (4): 1353–1404. https://doi.org/10.1103/RevModPhys.81.1353.

Mott-Smith, Harold M. 1971. “History of ‘Plasmas.’” *Nature* 233 (5316): 219–219. https://doi.org/10.1038/233219a0.

Nardin, Corinne, and Helmut Schlaad. 2021. *Biological Soft Matter: Fundamentals, Properties, and Applications*. Newark, GERMANY: John Wiley & Sons, Incorporated. http://ebookcentral.proquest.com/lib/bayloru/detail.action?docID=6524946.

Nefedov, Anatoli P., Gregor E. Morfill, Vladimir E. Fortov, Hubertus M. Thomas, Hermann Rothermel, Tanja Hagl, Alexei V. Ivlev, et al. 2003. “PKE-Nefedov*: Plasma Crystal Experiments on the International Space Station.” *New Journal of Physics* 5 (1): 33. https://doi.org/10.1088/1367-2630/5/1/333.

Nosenko, V., M. Pustylnik, M. Rubin-Zuzic, A. M. Lipaev, A. V. Zobnin, A. D. Usachev, H. M. Thomas, et al. 2020. “Shear Flow in a Three-Dimensional Complex Plasma in Microgravity Conditions.” *Physical Review Research* 2 (3): 033404. https://doi.org/10.1103/PhysRevResearch.2.033404.

Pekarek, L. 1968. “Ionization Waves (Striations) in a Discharge Plasma.” *Soviet Physics Uspekhi* 11 (2): 188. https://doi.org/10.1070/PU1968v011n02ABEH003809.

Piel, Alexander. 2017. “Molecular Dynamics Simulation of Ion Flows around Microparticles.” *Physics of Plasmas* 24 (3): 033712. https://doi.org/10.1063/1.4978791.

Pustylnik, M. Y., M. A. Fink, V. Nosenko, T. Antonova, T. Hagl, H. M. Thomas, A. V. Zobnin, et al. 2016. “Plasmakristall-4: New Complex (Dusty) Plasma Laboratory on Board the International Space Station.” *Review of Scientific Instruments* 87 (9): 093505. https://doi.org/10.1063/1.4962696.

Pustylnik, M. Y., B. Klumov, M. Rubin-Zuzic, A. M. Lipaev, V. Nosenko, D. Erdle, A. D. Usachev, et al. 2020. “Three-Dimensional Structure of a String-Fluid Complex Plasma.” *Physical Review Research* 2 (3): 033314. https://doi.org/10.1103/PhysRevResearch.2.033314.

Selwyn, G. S., J. Singh, and R. S. Bennett. 1989. “In Situ Laser Diagnostic Studies of Plasma-generated Particulate Contamination.” *Journal of Vacuum Science & Technology A* 7 (4): 2758–65. https://doi.org/10.1116/1.576175.

Smith, Bradford A., Laurence Soderblom, Raymond Batson, Patricia Bridges, Jay Inge, Harold Masursky, Eugene Shoemaker, et al. 1982. “A New Look at the Saturn System: The Voyager 2 Images.” *Science* 215 (4532): 504–37. https://doi.org/10.1126/science.215.4532.504.

Spitzer, Lyman, Jr. 1941. "The Dynamics of the Interstellar Medium. I. Local Equilibrium." *The Astrophysical Journal* 93 (May): 369. https://doi.org/10.1086/144273.

Thomas, H., G. E. Morfill, V. Demmel, J. Goree, B. Feuerbacher, and D. Möhlmann. 1994. "Plasma Crystal: Coulomb Crystallization in a Dusty Plasma." *Physical Review Letters* 73 (5): 652–55. https://doi.org/10.1103/PhysRevLett.73.652.

Tonks, Lewi. 1967. "The Birth of 'Plasma.'" *American Journal of Physics* 35 (9): 857–58. https://doi.org/10.1119/1.1974266.

Vermillion, Katrina, Dustin Sanford, Lorin Matthews, Peter Hartmann, Marlene Rosenberg, Evdokiya Kostadinova, Jorge Carmona-Reyes, et al. 2022. "Influence of Temporal Variations in Plasma Conditions on the Electric Potential near Self-Organized Dust Chains." *Physics of Plasmas* 29 (2): 023701. https://doi.org/10.1063/5.0075261.

Vermillion, Katrina, Abbie Terrell, Emerson Gehr, Evdokiya G. Kostadinova, Peter Hartmann, Lorin S. Matthews, and Truell W. Hyde. n.d. "Numerical Modeling of the Plasmakristall-4 Experiment on the ISS." In *AIAA SCITECH 2023 Forum*. American Institute of Aeronautics and Astronautics. Accessed January 30, 2023. https://doi.org/10.2514/6.2023-1587.

Vorona, N. A., A. V. Gavrikov, A. S. Ivanov, O. F. Petrov, V. E. Fortov, and I. A. Shakhova. 2007. "Viscosity of a Dusty Plasma Liquid." *Journal of Experimental and Theoretical Physics* 105 (4): 824–30. https://doi.org/10.1134/S1063776107100172.

"What Is Plasma? - Health Encyclopedia - University of Rochester Medical Center." n.d. Accessed January 25, 2023. https://www.urmc.rochester.edu/encyclopedia/content.aspx?ContentTypeID=160&ContentID=37.